A Model Potential Approach to Charge Resonance Phenomena in Aromatic Cluster Ions

Benjamin Bouvier,* Valérie Brenner, Philippe Millié, and Jean-Maïk Soudan

CEA Saclay, DSM/DRECAM/SPAM, Laboratoire Françis Perrin, URA 2453, Bât. 522, 91191 Gif-sur-Yvette, France

Received: March 20, 2002; In Final Form: July 30, 2002

This work proposes a simple yet accurate methodology to account for charge resonance in ionic clusters. The supersystem's model Hamiltonian is described via a basis set of valence bond structures for which the charge is localized on a given monomer, and whose intermolecular binding energies are computed using a polarizable model potential. The coupling elements between these structures are proportional to an overlap integral between relevant nonorthogonal monomer molecular orbitals. Ab initio calculations are employed to calibrate and validate the model, but also to define its limits. The methodology is then applied to the global exploration of potential energy surfaces for small homocluster ions of benzene, naphthalene, and anthracene. The structural and electronic properties of these systems are discussed, with emphasis on important trends such as the polarization vs charge-transfer competition or the difference between adiabatic and vertical ionization potentials. Extensions to stacked cluster ions of higher aggregation number ($n = 15$) conclude this work.

I. Introduction

Molecular clusters of aromatic compounds have been the subject of ongoing experimental and theoretical studies for a long while. They provide valuable insight for the comprehension of π interactions,[1] which play a predominant role in phenomena such as stacking or π hydrogen bonding.[2,3] Since aromatic moieties are present in many large organic molecules and biopolymers and often play an important part in noncovalent interactions, this knowledge can be fruitfully extended to the comprehension of local or group-wise phenomena. Although less effort has been invested in the study of charged aromatic clusters than in their neutral counterparts, it is now well-established that, for small aggregation numbers, their structural and electronic properties are very different from those of the neutral aggregates. This is evidenced by the important gap between the adiabatic and vertical ionization energies, and can be explained by the dominating influence of charge-transfer interactions. Hence, small aromatic clusters are ideally suited as model systems for the study of charge resonance phenomena.

However, the apparent chemical simplicity of small aromatic clusters conceals the theoretical difficulties which ab initio calculations run into when applied to these systems. First of all, typical near-neighbor interaction energies in neutral clusters amount to less than 2 kcal/mol, that is, require very accurate (and costly) ab initio calculations. Additionally, this interaction originates from subtle tradeoffs between dispersion, repulsion, and electrostatic energy contributions, whose relative importance may vary drastically depending on the cluster structure. Particularly delicate among these interactions are the dispersion effects, based on electron correlation and whose convergence with regard to basis set size is quite slow.[4,5]

The most striking example of these difficulties occurs in the case of the neutral benzene dimer, which has undergone extensive theoretical study. The Hartee−Fock (HF) level of calculation yields a repulsive interaction energy.[6] At the Møller−Plesset second-order perturbation theory level (MP2), the attractive nature of the interaction is correctly rendered, but systematically overestimated.[7,8] It is common knowledge that density functional (DFT) calculations often provide unreliable dispersion energies; hence, applying DFT advisably to these systems requires an additional dispersion potential.[9] On the whole, only expensive coupled-cluster calculations including single, double and perturbative treatment of triple excitations from the ground state (CCSD-T) can be said to yield accurate results.[10]

A different type of problem is encountered when studying small charged aromatic clusters. Typical pairwise interaction energies are 1 order of magnitude greater than for neutral aggregates, ensuring much smaller relative errors. The nature of the interaction is also significantly different, consisting, to a large extent, of polarization and charge resonance terms. However, the description of charge resonance phenomena by molecular orbital-based theories (MO) is biased by the method itself: a homodimer bearing a global +1 charge will favor symmetric solutions at short range and dissymmetric ones at longer distances, the occurrence of the symmetry-breaking artifact depending on the system and the method; discontinuity and instability can take place at the border separating the two zones.[11,12] Clearly, monodeterminantal approaches such as HF or HF-based methods are frequently plagued by this problem, but virtually all methods involving a self-consistent field procedure, whether mono- or multireferential, can also be affected. As a rule of thumb, the artifact has to be considered as soon as the correct description of the system requires more than one Lewis structure. For such a case, the valence bond (VB) theory sounds very appealing indeed, but generalized valence bond approaches rapidly become cumbersome as the system grows larger. Finally, let us mention that DFT, although not strictly speaking a molecular orbital method, does not offer a better description of charge resonance interactions.[13] On the whole, the process of selecting a reliable ab initio method for a given system featuring charge-transfer cannot be systematized

* Corresponding author. Phone: +33-1-6908-3788. Fax: +33-1-6908-8707. E-mail: bouvier@pandora.saclay.cea.fr.

10.1021/jp025794d CCC: $22.00
Published on Web 10/08/2002

and, more often than not, resorts to choosing elaborate methods that are unsuitable for large systems.

The aforementioned problems are by no means trivial; in this context, model potential methods are very attractive. For neutral aromatic clusters, their absolute error margins are comparable to those of ab initio calculations, at a tremendously lower computational cost. Combined with a VB method, they should provide a physically coherent approach to the study of charge resonance phenomena in charged aggregates. Possible applications of these relatively inexpensive methods vary from the global exploration of potential energy surfaces to molecular dynamics calculations.

Model potentials calculations have already been carried out on small neutral aromatic clusters,[14−18] but to our knowledge, no such potential has been able to tackle the case of ionized clusters. Furthermore, although methodologies ensuring description of charge-transfer phenomena have already been utilized in other systems (most relevant among which that of Jortner et al in DNA strands[19−21]), they are currently restricted to static geometries.

The present work proposes to address the question using a VB-based charge resonance-inclusive model potential supporting potential energy surface (PES) exploration techniques. In a first part, the methodology used to construct and calibrate the potential is explained. Then, the ab initio method selected as the calibration reference is discussed. Once correctly parametrized, the potential is applied to the thorough exploration of the PES for small charged and neutral homoclusters of benzene, naphthalene and anthracene, with aggregation numbers up to $n = 4$. Structural properties of the charged and neutral clusters are compared, with a focus on the implications of the charge resonance vs polarization competition, as well as on the adiabatic and vertical ionization potentials. The spatial delocalization of the charge in ionized clusters is also investigated. Finally, columnar aggregates of these compounds are investigated up to $n = 15$, providing valuable insight into charge delocalization processes in larger systems.

II. Methodology

II.1. Effective Hamiltonian and Valence Bond Framework. The energy and wave function of an *n*-molecular system bearing a global +1 charge are defined as the eigenvalues and eigenfunctions of an effective Hamiltonian matrix, built using a straightforward VB formalism; this procedure has already been applied to the study of charge-transfer effects in small water−ion clusters.[22] We shall discuss the formalism in the simplest case where the charged cluster is denoted $(M_1M_2...M_n)^+$, and each individual molecule M_i is characterized by a neutral form M_i and a ionic form M_i^+. The functions $\{(M_1M_2...M_i^+...M_n), i \in \{1...n\}\}$, form a basis set which underlies the effective Hamiltonian matrix, i.e., the wave function of the globally charged aggregate is written out as a linear combination of states where the charge is localized on a given molecule, all other entities being in their respective neutral ground states. The diagonal elements of the effective Hamiltonian matrix represent the energies of the aforementioned states. The off-diagonal elements coupling two of these mesomer forms are the direct translation of the charge-transfer phenomenon, and can be viewed as an extension to molecular systems of the "hopping integral" formalism in wide use among solid state physicists. They act as a link between the electronic structure of the monomers, which is known, and that of the cluster, which is not. This effective Hamiltonian approach has the advantage of modeling charge transfer as a many-body term, which is effectively the case in near-resonant cases for which two-body or perturbative treatments fall short of the mark.[23] Additionally, when evaluating diagonal elements, full knowledge of the state (neutral or charged) of each molecule is accessible, so that it should be possible to treat these two states at a different calculation level altogether (i.e., by maintaining different model potential parameter sets for each species).

II.2. Energy of the Valence Bond Structures. The energy of the VB structures, i.e., the diagonal elements of the effective Hamiltonian matrix, are evaluated using an enhanced[24−26] version of the intermolecular polarizable model potential of Claverie and Vigné-Maeder.[27,28] An extensive description of the potential being beyond the scope of this text, only a brief outline is given hereafter.

The potential assumes intramolecular geometries to be frozen and describes each molecule by six degrees of freedom (three translations and three Euler angles). On the basis of the exchange perturbation theory, it contains terms corresponding to the electrostatic, dipole polarization, dispersion, repulsion, and exchange dispersion energy contributions.

The electrostatic energy originates from the interaction between multipolar (up to the quadrupole) multicenter (atoms and bond centers) distributions on each molecule, which are derived from an ab initio one-electron density matrix calculation at a requisite level, followed by a site reduction procedure.

The dipole polarization energy results from a self-consistent iterative procedure during which additive site polarizabilities on each molecule respond to the electric field created by the (permanent and induced) moments on all other molecules. Thus, the polarization energy is not merely treated as a many-body term, but the influence of back-polarization is also taken into account. In the original work of Claverie, site polarizabilities are calculated using an additive bond-polarizability model developed by Lefevre,[29] in which each bond is affected a parallel and a perpendicular component depending on its type, with the notable difference that those two parameters are combined in a mean isotropic site polarizability. This is clearly unsuitable for aromatic moieties whose polarizability anisotropy is high (ca. 53% for benzene[30]). Restoring the full site polarizability tensor using Lefevre's parameters does not suffice, since a single perpendicular bond component is insufficient to account for the out-of-plane polarizability of aromatics. Separation of the π and σ subsystems (each with its own set of three bond parameters: one parallel, one in-plane perpendicular, and one out-of-plane perpendicular) is a baseline requirement for such systems, as has been explained by Mulder.[31] An enhanced version of Mulder's parametrization, designed to yield realistic site polarizabilities (the original scheme only aims at reproducing molecular tensors and anisotropies) was used for this study; it shall be the object of a forthcoming communication.[32] Polarization energy, albeit small in neutral aromatic clusters, acts as a counterbalance against delocalization in charged clusters, as shall be seen hereafter; correct description of this contribution is therefore essential.

The dispersion, repulsion, and exchange dispersion contributions are approximated as a sum of atom−atom terms using a Kitaigorodski[33] formalism, in which individual atom types are defined by two parameters. Three different distance zones, using distinct analytical formulas, are governed by these parameters. This ensures a realistic treatment of short-range terms (i.e., penetration effects), while still providing continuity and derivability at the border between the zones. However, the implied interdependence between the domains is a drawback when adjusting the potential parameters, as shall be seen shortly.

II.3. Implementing Charge Transfer. *II.3.1. General Framework.* As mentioned earlier, the off-diagonal matrix elements coupling two distinct VB structures are responsible for charge resonance inside the cluster. Assuming each of these VB structures to be fairly described by a zeroth-order wave function $|\Psi_i\rangle$, $i \in \{1...n\}$, built on the same set of mutually orthogonal supersystem molecular orbitals that are localized on each of the monomers (vide infra), the coupling element between VB structures i and j, $i \neq j$, may in all cases be expressed as a Fock operator matrix element defined by

$$\langle \Psi_i|H|\Psi_j\rangle = F_{kl} = \langle \varphi_k|F|\varphi_l\rangle \tag{1}$$

where φ_k and φ_l refer to the two localized molecular orbitals involved in the electron transfer, i.e., $|\Psi_j\rangle = a^+_k a_l|\Psi_i\rangle$. However, the prohibitive cost of constructing a Fock operator for each configuration or time step in Monte Carlo or molecular dynamics simulations calls for a simpler way of evaluating the off-diagonal elements of the effective Hamiltonian. This is most easily achieved by utilizing the popular linear relationship between these elements and an overlap integral between a suitably chosen pair of (nonorthogonal) neutral monomer molecular orbitals χ_p and χ_q:

$$\langle \Psi_i|H|\Psi_j\rangle = K_{pq}\langle \chi_p|\chi_q\rangle \tag{2}$$

The proportionality factor K_{pq} depends a priori on the system's nature, its geometry, and the molecular orbitals involved in the overlap. However, inside sets of cluster geometries, the ratio of the coupling element over the overlap integral (eq 2) is nearly constant, so that the aforementioned geometry dependence may often be safely ignored. This additional level of approximation will be detailed further on.

It is a reasonable assumption to suppose that the coupling element H_{ij} depends on the nature of the monomers involved in the charge-transfer mechanism (i.e., the monomers bearing the charge in valence bond structures Ψ_i and Ψ_j) but not on the other molecules in the aggregate. The coupling element is thus defined as a two-body term, while many-body effects are included in the diagonal elements of the Hamiltonian (the intermolecular interaction energies of the corresponding valence bond structures). Hence, for a given pair of monomers, the parameter K can be inferred from ab initio calculations on the dimer, and used as-is in model potential calculations on larger clusters featuring the same monomer pair, regardless of the nature of the other molecules.

Finally, molecular orbital dependence is not much of an issue if a single ionization involving a single MO (generally the highest occupied one) is considered per monomer unit. Extension to more complex cases will also be discussed hereafter.

We attempt to characterize charge-transfer interactions in a given system using the aforementioned proportionality factor K as the sole parameter. Its determination from ab initio calculations is explained in the following paragraph.

II.3.2. Ab Initio Parameter Determination and Validation. As seen earlier, correct inclusion of charge-transfer effects in an ab initio calculation is by no means a simple task. Furthermore, using such a calculation as a calibration reference for the model potential requires some degree of equivalence between the two levels, which should include or neglect the same effects. The procedure is detailed in the simple case of two monomers for which the ionization occurs on a single MO, and is extended to species where more than one MO has to be explicitly considered. Let us stress the fact that the procedure provides a value of the parameter K for a given cluster geometry only, and needs to be iterated over a set of cluster structures before a mean value for K can be found.

A Hartee−Fock calculation is carried out for both neutral monomers (monomer geometries inside the complex are considered equivalent to those of the isolated molecules). The molecular orbital involved in the ionization is identified. Another Hartee-Fock calculation is then applied to the neutral dimer. The combined set of occupied monomer orbitals is projected onto the occupied set of dimer molecular orbitals, resulting, after orthonormalization, in a set that is localized on each of the molecules but preserves intramolecular delocalization. This is a requisite to transcription of the aromaticity of the molecules, which stems from π electron delocalization: it justifies our choice of the aforementioned projection method compared to other popular localization schemes.[34] The same procedure yields a set of localized virtual orbitals from monomer and dimer virtual MOs.

Description of a VB limit-structure using a single determinant constructed on these orbitals leaves out the major part of polarization effects. We chose to render these effects using a selected CI approach. The polarization of the neutral monomer by the one bearing the charge is modeled by including all single excitations from the former's occupied orbitals to its virtual orbitals. Inclusion of all possible single excitations on the charged monomer (doubly occupied → virtual, doubly occupied → singly occupied, and singly occupied → virtual) transcribes the repolarization of the monomer's neutral orbitals under the effect of the charge. Charge-transfer interactions, which are taken care of in the off-diagonal terms, must not contaminate the diagonal elements; this is ensured by omitting any excitation involving orbitals located on different monomers.

Two such selected CIs are conducted, their respective first roots E_1 and E_2 yielding the energies of the two VB structures. Off-diagonal elements are written out as KS_{12}, where S_{12} is the overlap between the monomer MOs involved in the charge resonance:

$$H_{\text{eff}} = \begin{pmatrix} E_1 & KS_{12} \\ KS_{12} & E_2 \end{pmatrix} \tag{3}$$

A third CI, whose active space is obtained by concatenation of those of the two previous ones, provides the global system energy taking charge transfer into account. This calculation is used as a reference to calibrate the effective Hamiltonian formalism (eq 3). It is done by adjusting the parameter K so that the first root λ_1 of the global CI matches the lowest eigenvalue of the effective Hamiltonian; when this is verified, the second CI root λ_2 and the second eigenvalue of H_{eff} are generally very similar as well. This ensures that both the ground and the first excited state of the dimer ion (respectively associated with the first and second eigenvectors of the effective Hamiltonian) are correctly described using the current value of K. In the case of two strictly equivalent monomers ($E_1 = E_2$), the condition is fulfilled if $KS_{12} = {}^1/_2(\lambda_1 - \lambda_2)$, the first two CIs being rendered superfluous.

This procedure is iterated over a set of physically relevant geometries of the dimer cluster. For each of these, the coupling element is plotted versus the corresponding value of the overlap integral. A subsequent linear regression yields a mean value for the parameter K over the set. The choice of the dimer geometries forming the set is detailed in part III, on specific examples.

The procedure allows realistic treatment of charge-transfer and polarization effects, and is as comparable as can be with the model potential level of calculation that is used for the

diagonal energies. It should provide reliable estimates of the mean parameter *K*.

II.3.3. Extension: Multiple Ions. The aforementioned procedure may be extended to cases where the inclusion of more than one possible VB structure per charged monomer is necessary. This occurs for species that have several close-lying ionization potentials (IP), such as pyridine or toluene. The case of benzene, whose lowest ionized state involves two molecular orbitals, can be treated in the same manner by formally considering two degenerate states involving one singly occupied molecular orbital each. The effective Hamiltonian for a homodimer cluster with two IPs per monomer now takes the form

$$H_{\text{eff}} = \begin{pmatrix} E_1^{\,1} & 0 & V_{11} & V_{12} \\ & E_1^{\,2} & V_{21} & V_{22} \\ & & E_2^{\,1} & 0 \\ & & & E_2^{\,2} \end{pmatrix} \tag{4}$$

Successive ions on the same monomer are considered decoupled, while four off-diagonal elements V_{ij} bind ion i on the first monomer to ion j on the second. These are written in the form $V_{ij} = KS_{ij}$, where K is a mean parameter averaged on all possible (i,j) pairs.

Five CI calculations are now required. The global CI contains singly excited configurations built on four references (two different ions on two monomers). The diagonal element $E^a{}_i$ is the first root of a CI whose reference is ion a on molecule i. Since some active space overlap can occur between CIs for $E_i{}^a$ and $E_i{}^b$, $a \neq b$, some configurations have to be deleted from one of these calculations. As a rule of thumb, the concatenation of the four active spaces of the diagonal element CIs should coincide with that of the global CI.

Diagonalization of the effective Hamiltonian (eq 4) yields four solutions, the lowest of which is made to match the first root of the global CI by optimizing the value of K. As before, this results in a close agreement between the next three roots of the CI and the three remaining eigenvalues of the effective Hamiltonian, with the consequence that the ground state as well as the first three excited states of the ion cluster are correctly rendered.

The extension of the model to multiple ions per monomer implies an additional level of approximation compared to previously described cases. As mentioned earlier, the factor K is supposed to be specific to the pair of valence bond structures which it couples. In the case of single-ion monomers, there are as many valence bond structures as there are molecules, so that it is equivalent to say that K is specific to a pair of monomers. When multiple-ion monomers are considered, this is no longer true since more than one valence bond structure may correspond to the localization of the charge on a given monomer. For the sake of simplicity we chose to retain the monomer-pair dependence, at the cost of averaging K as mentioned above. Successes and failures of this model, applied to specific examples, are discussed in part III.

II.4. Potential Energy Surface Exploration. Our approach to charge transfer interactions features a sufficiently good tradeoff between precision and computational cost so as to allow real-time applications to systems of nonstatic geometries. This work will focus on global potential energy surface exploration.

The model potential energy surface for a given system is explored using a combination of three different methods: Monte Carlo growth (MCGM),[35−37] simulated annealing (SA)[38,39] and quasi-Newton optimization (QNO).[40] MCGM constructs a cluster monomer by monomer and generates a Boltzmann sample of configurations for each cluster size at a fictitious temperature T. Each monomer is contained inside a bounding sphere, which is tested for intersections against that of the newly added molecule, at each size step. Hence, the method reaches full efficiency for aggregates of molecules that are either small or grossly spherical.

Starting from random configurations, SA samples local attraction basins on the potential energy surface (PES) by using a Metropolis[41] algorithm associated with a controlled "temperature" parameter, which is decreased according to an annealing schedule. This algorithm gives a good global picture of the PES for all kinds of molecules, but the exponential rise of the number of local minima on complex or high-dimensional surfaces may render subsequent optimizations unfeasible.

QNO optimizes a given configuration by moving across the surface in a (downhill) direction given by an approximation of the inverse Hessian matrix, until a minimum is reached. This requires knowledge of the energy gradient at each step. The energy is the lowest eigenvalue of the H_{eff} matrix, i.e., the lowest element of diagonal matrix E defined by

$$E = {}^{t}AH_{\text{eff}}A \tag{5}$$

where A is the eigenvector matrix obtained by diagonalizing H_{eff}. H_{eff}, being a real symmetric array, gives a straightforward demonstration[42] that the derivative of E relative to variable X is

$$\frac{\partial E}{\partial X} = {}^{t}A\frac{\partial H_{\text{eff}}}{\partial X}A \tag{6}$$

The analytical derivation of the diagonal element of H_{eff} will not be discussed here. Derivation of the off-diagonal element KS requires the derivative of the overlap integral S; it can be shown that it is itself an overlap integral between Cartesian Gaussians whose quantum numbers n_x, n_y, and n_z differ from one unit.

Finally, the QNO subroutine numerically evaluates the Hessian after convergence, to ascertain the nature of the optimum (minimum or saddle point). Since QNO is a local method, it was used as a second step to global techniques such as MCGM and SA.

II.5. Computational Details. Monomer geometries were optimized at the B3LYP/cc-pVDZ[43] level using Jaguar 4.1[44] and refined at the MP2/6-311G(2d,2p)[45] level using Gaussian98.[46] Neutral benzene dimer calculations were performed at the counterpoise-corrected[47] MP2 and CCSD-T levels using the 6-311G(2d,2p) basis set in Gaussian98. Electrostatic multipole distributions were obtained by a one-electron MP2 density calculation in this basis set. Selected CIs were carried out using HONDO95[48] and CIPSI,[49,50] with a 6-31G*[51] basis set. CASPT2 calculations on pyridine systems were done using Molcas 5.0[52] and basis set aug-cc-pVDZ.[43] Model potential calculations as well as PES explorations were performed using software designed in the laboratory. All calculations were run on a Compaq ES40 AlphaServer and two Silicon Graphics O200 workstations.

III. Ab Initio Modeling of Charge Transfer

The model, which allows adequate values of the parameter K to be inferred from ab initio selected CI calculations, was applied to several homodimer clusters. Ethylene and naphthalene were described using the single-IP formalism, the former as a

TABLE 1: Typical Center-of-mass Distances, Coupling Elements, and Mean *K* Values for Sets of Relative Geometries of an $(Ethylene_2)^+$ Cluster[a]

symmetry operation	initial disposition	typical distances (Å)	typical coupling element (au)	*K* (au)
$C_2(z)$ translation	stacked	2.5−7.0	7×10^{-2}−7×10^{-6}	0.308
$C_2(z)$ rotation	stacked	3.3	10^{-2}	0.351
	stacked	5.0	10^{-3}	0.483
$C_2(z)$ rotation	coplanar	5.0	10^{-3}−10^{-4}	0.538
$C_2(x)$ rotation	stacked	5.0	10^{-4}−10^{-5}	0.676

[a] The sets are generated by applying a simple symmetry operation (a stepwise translation along or rotation about an axis) to one of the monomers of an initial cluster, while the other molecule is kept fixed. The initial cluster geometry is either stacked (the second monomer is deduced from the first by a translation along the $C_2(z)$ axis) or coplanar (the second monomer is deduced from the first by a translation along the $C_2(y)$ axis); both are of D_{2h} symmetry. Axes are named according to the symmetry elements of point group D_{2h}.

case study to validate the model, the latter as an extension to a larger species. For benzene and toluene, the multiple-IP scheme was employed and tested. Finally, the study of pyridine yielded valuable insight into the limits of the mean *K* approximation.

III.1. A Case Study: Ethylene. Ethylene is the simplest molecule containing a π subsystem; hence, it is well suited as a case study of the previously discussed method. The first ionized form of ethylene is a $^2\Pi$ state. Coupling terms for charge transfer in an ethylene dimer will involve overlap between instances of these π-type monomer MOs.

From simple initial geometries of an $(ethylene)_2^+$ cluster (Table 1), sets of clusters were generated by allowing one molecule to undergo simple transformations (stepwise rotations along or translations about an axis), the other monomer being kept fixed. Inside each set, selected CI calculations were performed for each of the member clusters, and the resulting coupling element was plotted against the corresponding overlap value. A linear regression supplied the mean value of *K* over the set. Results are compiled in Table 1.

As can be seen, values of *K* vary much between cases. A general trend appears: when the coupling element H_{12} decreases (i.e., for long distances or near-orthogonal MOs), the value of *K* has to be increased to verify $H_{12} = KS$. This explains that the different sets, involving different magnitudes in overlap and/or coupling, feature different mean *K* values. We infer that the linear dependence of H_{12} on *S* is not rigorous, and may only be achieved inside given ranges of *S*. This problem could possibly be circumvented by maintaining different values of *K* for different overlap magnitudes, or by selecting the value of *K* that is typical of the structures under study. Neither solution is practical, however, when it comes to global exploration of a potential energy surface. Another issue concerns the $\sigma-\pi$ mixing which occurs for homodimer geometries where the planes of both monomers are nearly orthogonal. In such cases, the $\pi-\pi$ overlap (which monitors charge transfer in our model) vanishes, while the coupling element, albeit small, persists (because of limited $\sigma-\pi$ coupling which our model is unable to transcribe). This results in an altogether nonlinear relationship between H_{12} and *S*.

To ascertain the order of magnitude of the error introduced by the mean *K* approximation, we resorted to a more statistical approach: 500 distinct homodimers were randomly generated, with the constraints that (i) the center-to-center distance between monomers be smaller than 7.5 Å and (ii) the two monomers' bounding boxes (i.e., parallelepipeds enclosing the molecules' van der Waals spacefill) do not intersect. This provided a good

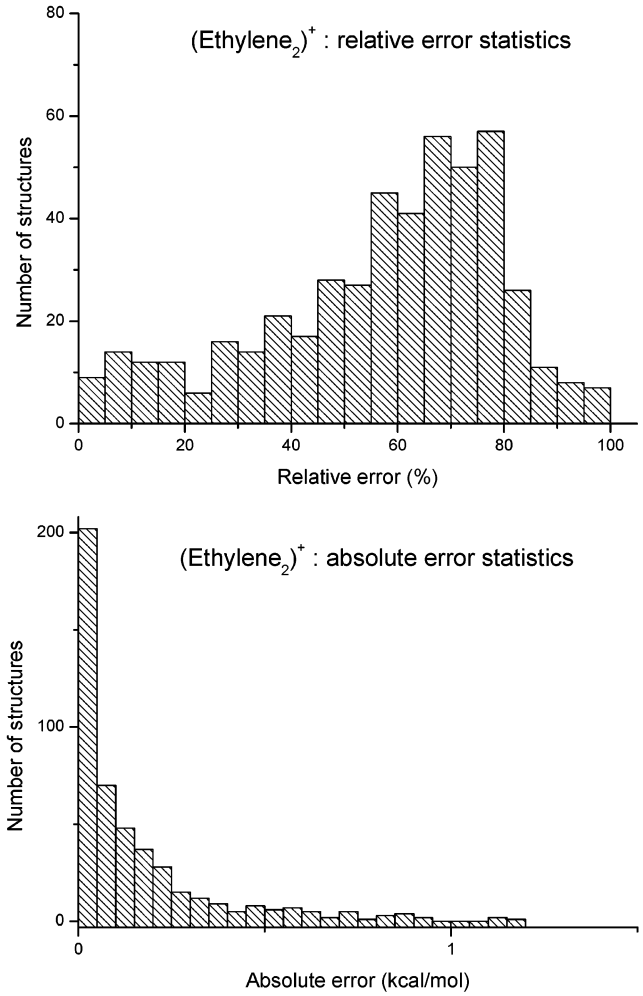

Figure 1. Absolute and relative error statistics of the determination of the off-diagonal coupling element using the mean *K* approximation, for 500 random $(ethylene_2)^+$ geometries, with selected CI calculations as a reference.

sampling of the PES, with coupling values between 10^{-1} and 10^{-6} au. The mean value of *K* for this series ($K_{mean} = 0.361$ au) was determined, and the error evaluated for each geometry by comparing $K_{mean}S$ to the corresponding ab initio coupling. Absolute and relative error histograms appear on Figure 1. The difference between both graphs is striking: the relative error, albeit very small (<0.1%) for large values of *S*, can reach ca. 100% in some cases. On the contrary, the absolute error is always small and, with a mean value of 0.2 kcal/mol, is comparable to the precision of the model potential used for the diagonal terms of the Hamiltonian. This is of course due to the fact that high-overlap configurations contribute most significantly to the fit: K_{mean} is adequate to describe high-overlap configurations but fails for low-overlap ones. However, since these involve very small coupling elements, the absolute error remains acceptable in all cases.

Selected CI calculations do not scale favorably when the number of basis functions grows, preventing statistical studies on bigger systems. Considering the aforementioned trends as general, we will infer values of *K* from high-overlap homodimers in forthcoming systems (mostly stacked isomers in our case).

Finally, we investigated the basis set dependence on the value of *K*. From a reasonable number of basis functions on, basis set size has almost no influence on the coupling element H_{12}, in good agreement with Jortner's finding.[20,21] However, the

convergence of overlap integrals between molecular orbitals with basis set size generally occurs at larger basis dimensions. This apparent discrepancy is corrected by the choice of *K*: for a given cluster geometry, larger basis sets will generally give rise to larger overlap integrals but to lower values of *K*, while smaller basis sets will compensate for the underestimation of *S* by a higher value of *K*, in such a way that the coupling value (i.e., the product *KS*) remains almost constant. This has two practical consequences: (i) the basis set used for the selected CI calculations from which *K* is inferred should be of sufficient quality to ensure correct transcription of the coupling element (most particularly the influence of polarization effects on the latter) and (ii) this same basis set is to be employed for the determination of overlap integrals in subsequent model potential computations, along with the corresponding value of *K*. The basis set 6-31G* was found to verify these two conditions for the aromatic clusters under study, while still compatible with cost-effective selected CI calculations.

III.2. Application: Naphthalene. Naphthalene and ethylene both have in common a single low-lying ionization potential, and are similarly described in the framework of our model. Selected CIs on the naphthalene dimer are very costly, but can be alleviated by restricting the active space to the π subsystem. This amounts to neglecting the reorganization of the σ subsystem, which has negligible effect when no σ-π mixing occurs, as is the case for stacked dimers (at least if the interplane distance is sufficiently large). Fitting sets were generated as for ethylene, by applying simple stepwise rotations and translations to high-overlap stacked homodimers. The mean value of K over the sets was found equal to 0.306 au, and was used for anthracene as well, since reasonably large selected CI calculations on anthracene are not feasible (due to high computational cost and basis size limitations inherent to the computer programs).

III.3. Multiple Ionized Forms: Toluene and Benzene. When two or more molecules interact, their respective states are split by a value ranging from twice the coupling (for two identical moieties) to four times the coupling (in the case of an infinite number of identical monomers giving birth to a band structure). Hence, the split can give rise to band mixing phenomena if two or more states are closer in energy than half the sum of their splitting values. In such a case, correct description of the system requires the inclusion of these states.

Toluene has two close-lying IPs, experimentally[53] located at 8.83 and 9.36 eV and involving the highest occupied molecular orbital (HOMO) and the one just below (HOMO-1), respectively. Both correspond to $^2\Pi$ states. Ab initio selected CIs are carried out as mentioned earlier. The mean parameter *K*, which is averaged not only on different cluster geometries but on the four different types of overlap integrals, equals 0.281 au. For most clusters structures, this additional level of approximation does not deteriorate the quality of the fit. The necessity to include two IPs per monomer clearly appears on Figure 2, which represents the contribution of each monomer ion to the charged supersystem ground state for two stacked parallel molecules, one of which is rotated around an axis perpendicular to both molecular planes and joining the two entities' centers of mass (because the center of mass does not coincide with the center of the aromatic ring, the monomers are symmetry-inequivalent). Depending on the rotation angle, relative contributions of HOMO and HOMO-1 can vary drastically.

Although benzene is characterized by a single low-lying IP involving two degenerate MOs (HOMO and HOMO-1, both of π type), it can formally be viewed as having two degenerate IPs involving one molecular orbital each, and is treated like toluene in the current model. The mean *K* value for the $(benzene_2)^+$ system is 0.258 au.

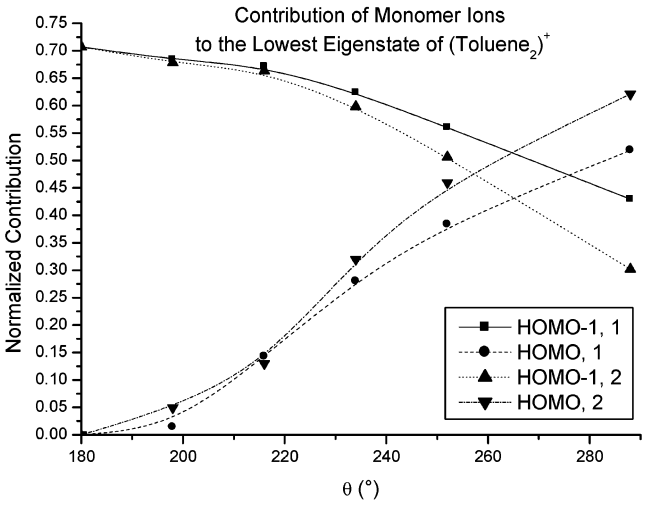

Figure 2. Normalized contributions of each monomer's two lowest ionized states to the ground-state electronic wave function of a stacked $(toluene_2)^+$ cluster, as a function of the rotation angle θ of the second monomer around the stack axis (which joins the two molecules' centers of mass). At $\theta = 0°$, the second monomer is deduced from the first by a 3.5 Å translation along this axis. The contributions are the coefficients of the monomer states in the normalized supersystem eigenvector. Monomer states are denoted by a reference to the molecular orbital where the ionization takes place (HOMO or HOMO-1, cf. text) and by the index of the monomer (1 or 2).

III.4. Limits of the Mean *K* Approximation: Pyridine. The case of pyridine is a particularly difficult one. This molecule has three close-lying IPs inside a 1 eV range. Two π-character ions may result from an ionization inside the π subsystem, whereas the ionization of the nitrogen nonbonding orbital generates a σ-character ion. There is much experimental[53−57] as well as theoretical[53,57] controversy regarding the correct ordering of these three states[53−57] and the nature of the lowest one.

The study of the charged pyridine dimer in our model raises an additional difficulty compared to benzene derivatives. The effective Hamiltonian for the pyridine dimer is built upon six distinct valence bond structures and features nine coupling elements (as before, successive ions on the same molecule are considered decoupled). We will restrict our discussion to the case of two equivalent pyridine monomers of coplanar geometry, with the nitrogen atoms facing each other (point group D_{2h}). In this configuration, the σ-nonbonding and π MOs on each monomer are orthogonal to each other, so that we need not preoccupy ourselves with $\sigma-\pi$ mixing phenomena. However, a single value of *K* must still be able to simultaneously account for the five remaining coupling elements governed by $\sigma-\sigma$ and $\pi-\pi$ overlaps, which may differ by several order of magnitude. We shall now investigate whether this is the case.

The pyridine monomer's molecular orbitals are representations of the C_{2v} point group. The three highest occupied MOs of neutral pyridine (two π-type and one σ-type, in decreasing energy order) are involved in the three ionic forms mentioned above. Their characters are a_2, b_1. and a_1, respectively. In turn, the planar pyridine dimer belongs to point group D_{2h}. Its six highest occupied MOs are easily identified as pairwise combinations of each of the monomers' three highest occupied MOs, each of these yielding a *gerade*/*ungerade* pair; all of these dimer

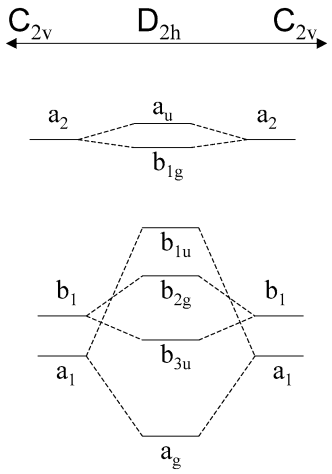

Figure 3. Schematic molecular orbitals correlation diagram showing the relationship between the three highest MOs of the neutral C_{2v} pyridine molecule (left and right) and the six corresponding MOs of the neutral D_{2h} pyridine dimer (center). For the sake of lisibility, state energies and coupling values are not quantitatively represented. Refer to Tables 2 and 3 for exact values.

TABLE 2: Ionization Potentials (eV) of the Pyridine Molecule at Two Different Levels of Theory[a]

	$E(^2A_2)$	$E(^2B_1)$	$E(^2A_1)$
CASPT2 π	9.53	10.24	not available
ROMP2	9.39	10.05	9.38

[a] As a comparison, the first IP of pyridine is experimentally[53] located at 9.60 eV

orbitals belonging to a different symmetry class, no mixing occurs. The relationship between the corresponding ionic states are shown on Figure 3. The charge-transfer coupling element for a given pair of monomer states can be considered equal to half the difference between the resulting *g*/*u* dimer state energies. We may now check whether the three coupling elements are proportional to a relevant overlap integral, and if a mean proportionality factor is sufficient to account for all three.

The energy of the monomer π-type ions ($^2A_2$ and $^2B_1$) were obtained by a CASPT2 calculation using the π subsystem as the active space (five electrons in six orbitals). The same was done for the neutral molecule. However, such a method cannot be applied to the σ-type ($^2A_1$) ion since it would require inclusion of the entire σ subsystem in the active space, which would de facto become prohibitively large. To be able to describe all ions at an equivalent level, we decided to check whether restricted open-shell MP2 calculations (ROMP2), modeled as a monodeterminantal CASPT2, would suffice. This approach yielded satisfactory results for the π-type ions, and was therefore applied to the σ-type one (Table 2). The experimentally postulated[56] accidental degeneracy between the $^2A_1$ and $^2A_2$ states is confirmed by these results.

The agreement between the CASPT2 and ROMP2 levels of theory was also noticed in the case of the D_{2h} pyridine dimer ion. ROMP2 calculations yielded the six possible ion energies. Coupling elements H_{12} were deduced as mentioned above; relevant MO overlap integrals between a_2, b_1, and a_1 MOs on each monomer were also evaluated. This procedure was iterated for N−N distances ranging from 2 to 4 Å; linear fit results of H_{12} vs S appear in Table 3. As predicted, the mean values for the three overlap integrals are very different and result in distinct K values. Even the two π-type overlaps differ of 1 order of magnitude (this is due to the fact that the b_1 MO has a contribution on the nitrogen atom, while the a_2 MO does not).

TABLE 3: Typical Molecular Orbital Overlap Integrals and Corresponding Mean K Values (au) for the Charged D_{2h} Pyridine Dimer, Depending on the Nature of the Monomer Ion (cf. Text)

	a_2	b_1	a_1
typical value of S (au)	10^{-3}	10^{-2}	10^{-1}
mean K (au)	0.349	0.289	0.402

The mean K approximation suffers from two different issues. First of all, one may infer from the case of pyridine that it is unable to simultaneously account for the coexistence of different charge-transfer interactions in a system, especially when different orbital types or distinct overlap ranges need be considered. Furthermore, the mean K value can differ significantly from species to species, even inside a given series of molecules displaying analogous properties (aromatics in our case). Hence, the method is expected to be much more reliable and easy to calibrate in homomolecular clusters than in heteromolecular ones.

IV. Charge Transfer in Aromatic Clusters: A Model Potential Study

Once determined, the value of K_{mean} allows the calculation of the off-diagonal coupling terms of the model Hamiltonian. In the same way, adequate parametrization of the model potential is required to evaluate the diagonal energies of the valence bond structures.

IV.1. Parametrization. The electrostatic contribution to the interaction energy is described via interacting multipolar multicenter distributions on the monomers. These are derived from an ab initio calculation and do not need to be adjusted. Parameters for the polarization contribution include anisotropic bond polarizabilities; these were fitted so as to reproduce (i) the experimental and ab initio molecular dipole polarizability tensor of benzene,[30] (ii) its anisotropy, and (iii) the medium-range interaction energy of benzene-containing dimers, which is due exclusively to electrostatic and polarization terms. Once these contributions were correctly transcribed, the dispersion−repulsion−exchange repulsion terms could be adjusted. This was done on the neutral benzene dimer (vide infra), for which a wealth of theoretical and experimental studies have been published, by acting on the four parameters of the aromatic carbon and hydrogen atoms. We used Hobza's counterpoise-corrected CCSD-T surface scans on stacked and T-shaped isomers,[10] which we complemented by several short-distance points using the same method and basis set.

This set of parameters was retained for all forthcoming studies on aromatic aggregates. Charged monomers were described using their own multipolar multicenter distribution, but with the same set of bond polarizabilities and dispersion−repulsion−exchange repulsion parameters than their neutral counterparts. Monomer ions were considered to share the same geometry as the corresponding neutral molecule, which is a good approximation in aromatics (despite a limited[58] Jahn−Teller effect in the benzene cation).

IV.2. Global Potential Energy Surface Exploration for Small Aromatic Clusters. Using the previously determined parameter set, a global potential energy surface exploration was carried out for small charged and neutral homoclusters of benzene, naphthalene and anthracene. While an extensive exploration is possible for dimer clusters, the number of isomers rapidly grows with the aggregation number in such a way that, for larger clusters, we mainly focused on the energetically low-lying conformations which we attempted to classify in structural families.

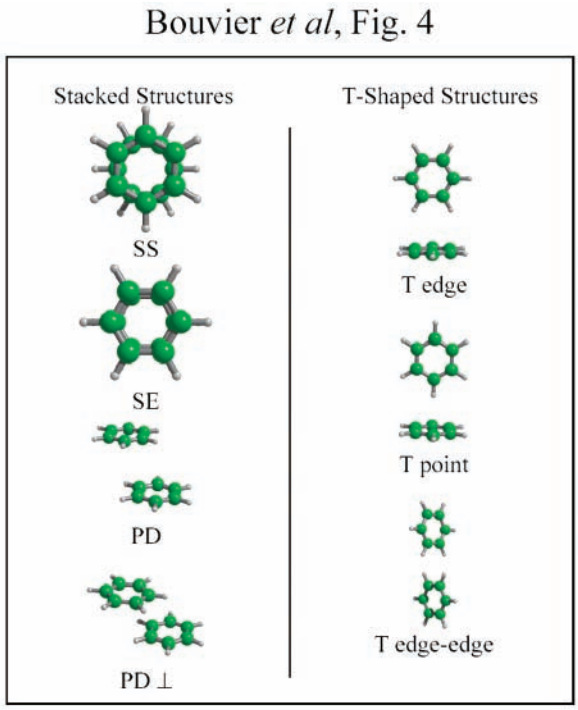

Figure 4. Generic structures of the stationary point of the $(benzene_2)$ and $(benzene_2)^+$ PES. The nature, the interaction energy and the geometric details of each structure are given in Tables 4 and 5 for neutral and charged clusters, respectively.

TABLE 4: Interaction Energies (E_{int}), Nature, and Typical Center-of-Mass Distances (R) of the Stationary Points on the Neutral Benzene Dimer Potential Energy Surface (Figure 4)

structure	E_{int} (kcal/mol)	nature	R (Å)
T-edge	−2.01	global minimum	4.93
T-point	−1.92	first-order saddle point	5.04
PD	−1.51	first-order saddle point	5.55
T-edge−edge	−1.49	minimum	6.01
SS	−0.98	second-order saddle point	3.94
SE	−0.98	third-order saddle point	3.94

TABLE 5: Interaction Energies (E_{int}), Nature, Typical Center-of-mass Distances (R), and Delocalized Character of the Stationary Points on the $(Benzene_2)^+$ Potential Energy Surface (Figure 4)

structure	E_{int} (kcal/mol)	nature	R (Å)	delocalized character (%)
SS	−26.05	global minimum	3.02	50/50
SE	−25.99	first-order saddle point	3.03	50/50
PD ⊥	−17.91	minimum	4.04	50/50
PD	−17.77	minimum	4.05	50/50
T-edge	−12.93	first-order saddle point	4.32	100/0
T-point	−12.41	second-order saddle point	4.27	100/0

Charged and neutral benzene dimer clusters were found to share common structure types, although the interaction energy, the nature (minimum or saddle point), and the center-of-mass distances of these structures may differ depending on the cluster charge. Figure 4 represents these generic structures, while Tables 4 and 5 give the nature, interaction energies and geometric details of each one for the neutral and charged benzene dimer cluster, respectively.

For the remaining clusters under study, the focus was set on minima rather than on saddle points. Since we usually found a clear dichotomy between neutral and charged structures, the corresponding figures (Figures 5−12) and tables (Tables 6−11) address the neutral and charged isomers separately.

IV.2.1. Neutral Benzene Dimer. The optimal structures obtained for the neutral benzene PES are detailed in Table 4. They can be classified into two categories: stacked and T-shaped (Figure 4). The T-shaped isomers are due to attractive electrostatic and dispersion interactions, whereas the stacked ones are electrostatically unfavorable and rely exclusively on attractive dispersion. Polarization interactions are in all cases very small. Total interaction energies are lower than 2 kcal/mol, which stresses the necessity for very accurate calculations.

The global minimum is a T-shaped structure, denoted "T-edge" (the edge of the first ring is parallel to the second ring's plane). Its center-to-center distance is very close to the experimental value of 4.96 Å.[59] A 30° rotation around the first molecule's center of mass yields the "T-point" isomer (a hydrogen atom of the first ring points toward the second ring's plane), which we identify as a first-order saddle point. In this respect, our calculation differs from other theoretical works[10] which find the T-point to be the global minimum and the T-edge to be a saddle point. This could result from subtle differences in the description of the quadrupole of benzene (necessarily less accurate than the dipole in our model, since the multipolar distribution is truncated at the quadrupolar term) and in the treatment of dispersion (especially concerning the hydrogen atoms). In any case, the two isomers are separated by a mere 0.09 kcal/mol (which is close to the precision of the potential), and unhindered rotation is expected to occur even at low temperatures, as stated by experimental intermolecular vibration studies.[60] Passim, we note the existence of another T-shaped structure, denoted "T-edge−edge", which has often been overlooked in previous works.

The stacked structures (SS and SE), generally less stable than their T-shaped counterparts, are saddle points (up to third order) rather than minima. The "parallel displaced" ones (PD) are usually lower in energy than the "sandwich" ones, due to less unfavorable electrostatics.

IV.2.2. Benzene Dimer Ion. The benzene dimer ion's optimal structures are detailed in Table 5. Although they belong to the same two classes as those of the neutral dimer (Figure 4), the stacked isomers are now much lower in energy than the T-shaped ones. For such stacked structures, the coupling elements of the model Hamiltonian may be up to twice as large as the diagonal interaction energies: interactions in the benzene dimer ion are governed by charge resonance. Hence, high-overlap configurations (e.g., stacked) will be favored. Analysis of the corresponding eigenvector show a perfect delocalization of the charge over the two monomers, whereas for T-shaped dimers (with overlap values close to nil), the charge is purely localized.

The "sandwich-staggered" (SS) structure is found to be the global minimum. The first-order saddle-point separating two SS structures, which we dub "sandwich-eclipsed" (SE), lies a mere 0.06 kcal/mol higher in energy (e.g., both conformations are degenerate to the precision of the model potential). This very weak energy difference is not due to charge resonance; during rotation around the axis joining the two monomers' centers of mass, compensations between the four types of overlap are such that the global charge-transfer interaction remains exactly constant. It is mainly due to the dispersion and electrostatic contributions to the diagonal energies. As was the case for the neutral T-shaped dimer, rotational disorder should occur in sandwich structures; this has been postulated by SCF calculations.[61] As far as geometry is concerned, a 1-Å shortening of the interplane distance occurs relative to the neutral sandwich isomer.

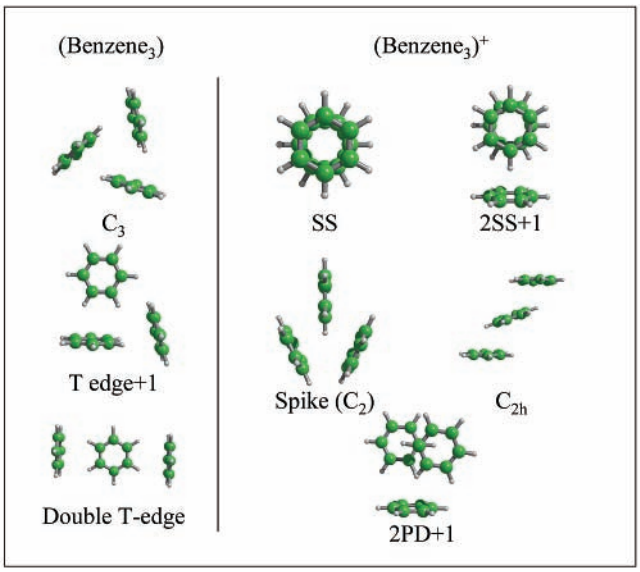

Figure 5. Structures of the most relevant minima on the (benzene$_3$) and (benzene$_3$)$^+$ PES (Tables 6 and 7).

The stacked nature of the global minimum, as well as the importance of charge resonance phenomena, was experimentally formulated in pioneering studies by Nishi et al.[62,63] and Hiraoka et al.[64] In these works, the binding enthalpies in the benzene dimer are estimated from −15 to −20 kcal/mol. Our calculation apparently overestimates this stabilization. The diagonal VB structures in stacked aggregates stem from an equilibrium between attractive polarization and (to a lesser extent) dispersion interactions on one hand, and repulsion on the other. The difference in interaction energy is probably due to an underestimation of the repulsive contribution: as already mentioned, repulsion and dispersion are fitted using the same set of atomic parameters, which in our case were calibrated on the neutral benzene dimer. Hence, our fit tends to favor the dispersive (long-distance) rather than the repulsive (short-distance) behavior. This problem is a recurrent one with our dispersion-repulsion model. It could possibly be solved by using a different set of parameters for the neutral and charged monomers, but for the sake of transferability, and for lack of convincing ab initio calculations on the benzene dimer ion, we chose to retain a unified version of the parameter set.

Finally, Nishi et al.[63] report a charge resonance band originating from the transition from the ground state of the dimer ion to the corresponding dissociative excited state. The corresponding photon energy is 1.3 eV (ca. 30 kcal/mol). Our model places the first dimer ion excited state at +13.295 kcal/mol, 39.3 kcal/mol higher than the ground state. The difference between experimental and theoretical figures is in fact probably not so large, because the experimentally detected excited state, being "hot", has a longer mean plane-to-plane distance than the ground state, resulting in a weaker coupling value, hence a smaller energy gap between the two states.

IV.2.3. Neutral Benzene Trimer. Three noteworthy minima were found on the neutral benzene trimer PES (Figure 5 and Table 6). Of these, only one is a typical three-molecule structure, whereas the others are derived from dimer geometries. This structure is actually the global minimum and features three equivalent benzene monomers; it belongs to point group C_3. Experimental evidence for such a global minimum has been provided by Raman studies.[65] The other two minima are built on the T-edge dimer structure and are differentiated by the position of the third benzene moiety (which interacts with both monomers in one case and with a single one in the other).

TABLE 6: Interaction Energies (E_{int}) of the Most Relevant Minima on the Neutral (benzene$_n$) PES, $3 \le n \le 4$ (Figures 5 and 6)

structure	E_{int} (kcal/mol)
C_3	−5.89
T-edge+1	−5.38
double T-edge	−3.90
C_2	−10.84
C_3	−9.89
C_1	−9.01

TABLE 7: Interaction Energies (E_{int}) and Delocalized Character of the Most Relevant Minima on the (Benzene$_n$) + PES, $3 \le n \le 4$ (Figures 5 and 6)

structure	E_{int} (kcal/mol)	delocalized character (%)
SS	−35.09	20/60/20
2SS+1	−34.39	50/50/0
spike (C_2)	−28.80	30/40/30
C_{2h}	−25.91	25/50/25
2PD+1	−25.03	50/50/0
3SS+1	−43.11	20/60/20/0
2SE+2T	−42.57	0/50/50/0
2SE+2V	−41.94	0/50/50/0
SS	−40.07	5/45/45/5
3 Spike+1	−36.45	30/40/30/0

IV.2.4. Benzene Trimer Ion. The global minimum on the benzene trimer ion PES (Figure 5 and Table 7) is a sandwich-staggered (SS) structure. As already mentioned, such stacked structures maximize charge-transfer interactions through overlap integrals; the SS structure's nature as global minimum implies the predominance of charge resonance for the benzene trimer ion. The structure is symmetric, the central unit bearing the greater part of the charge. Such a sandwich structure for the benzene trimer ion has been experimentally inferred[62] from π orbitals stabilization.

However, the influence of polarization is greater than in the dimer ion, so that it competes with charge-transfer interactions. It is the driving force of isomers such as the 2SS+1, the third benzene unit's placement maximizing this effect rather than charge resonance (which is restricted to the two stacked monomers). The same is true for isomer 2PD+1. The remaining two minima feature intermediate behaviors. From the fact that the SS and 2SS+1 structures are close in energy (0.7 kcal/mol), we infer that there is a close tie between charge resonance and polarization effects in the benzene trimer ion, which thus constitutes a frontier case in the (benzene$_n$)$^+$ series.

IV.2.5. Neutral Benzene Tetramer. Of the numerous stationary points on the neutral benzene tetramer PES (Figure 6, Table 6), only the global minimum, of point group C_2, features a characteristic four-coordinated structure. Higher minima are built on dimer and trimer motifs. Examples thereof are the C_3 isomer, as well as the frequently occurring C_1 structure.

There is experimental evidence for two types of symmetrically inequivalent sites[65] in the neutral benzene tetramer. An exp-6-1 model potential calculation by Van de Waal[66] proposes a tetrahedral cluster structure for which this is verified. However, our C_2 isomer also fits the experimental bill.

IV.2.6. Benzene Tetramer Ion. The charge resonance-polarization competition, whose onset was witnessed for the trimer ion, amplifies in the case of the tetramer ion: polarization of neutral moieties by charged ones now becomes the predominant term. As a consequence, charge delocalization for most minima on the benzene tetramer ion PES does not involve more than three molecules; these clusters stem from the addition of one or two neutral monomers to a (benzene$_2$)$^+$ or (benzene$_3$)$^+$ motif. The

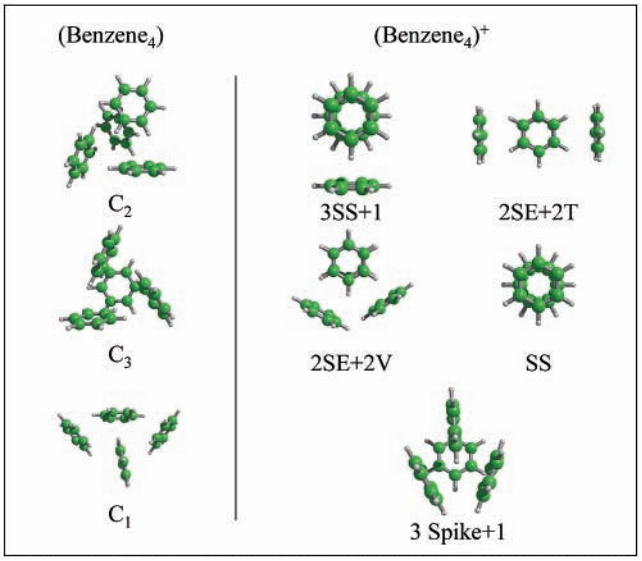

Figure 6. Structures of the most relevant minima on the (benzene$_4$) and (benzene$_4$)$^+$ PES (Tables 6 and 7).

TABLE 8: Interaction Energies (E_{Int}) of the Most Relevant Minima or Saddle Points (SP) on the Neutral (Naphthalene$_n$) PES, $2 \leq n \leq 4$ (Figures 7−9)

structure	E_{int} (kcal/mol)
T-point	−3.33
T-edge	−2.29
PD	−2.74
T-edge ⊥	−2.74
SS (first-order SP)	−2.48
SE (third-order SP)	−2.25
C_{3h}	−10.17
T-point+1	−7.74
double T-point	−6.66
C_1	−15.74
C_2	−15.49
C_{2h}	−15.46

only exception is the SS structure, where the charge spreads on all four monomers; although still a minimum, it is relatively high in energy, unlike the corresponding structure for the trimer ion.

Of the numerous stationary points found on the surface, the most relevant families are detailed on Figure 6 and in Table 7. The global minimum (3SS+1) is the combination of a (benzene$_3$)$^+$ sandwich-staggered structure and a neutral monomer, and features the best polarization−charge delocalization tradeoff.

IV.2.7. Neutral Naphthalene Clusters: Dimer through Tetramer. Global PES studies for neutral naphthalene dimer through tetramer aggregates were carried out. Results are compiled in Table 8, and in Figures 7−9. As for benzene, the naphthalene dimer global minimum is a T-shaped structure. Most other stationary points are reminiscent of those of (benzene$_2$), with the exception that, due to the lower symmetry of naphthalene, T-point isomers are generally more stable than T-edge ones. This does not come as a surprise, since dispersion and repulsion are the driving forces in these clusters. The trimer PES, in agreement with Raman experiments,[67] features a triangle-shaped C_{3h} structure as the global minimum. A triangle-shaped global minimum was also found for the neutral benzene trimer; however, the energy separation between this structure and subsequent local minima is more clear in the present case (2.5 kcal/mol compared to 0.5 kcal/mol for benzene). The double T-point structure mentioned by Wessel et al.[68] is also a minimum, albeit high in energy. Experimental data on the

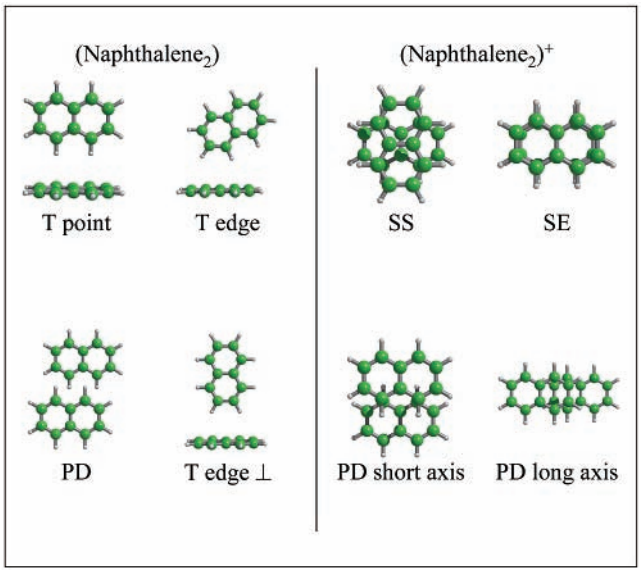

Figure 7. Structures of the most relevant stationary points on the (naphthalene$_2$) and (naphthalene$_2$)$^+$ PES (Tables 8 and 9).

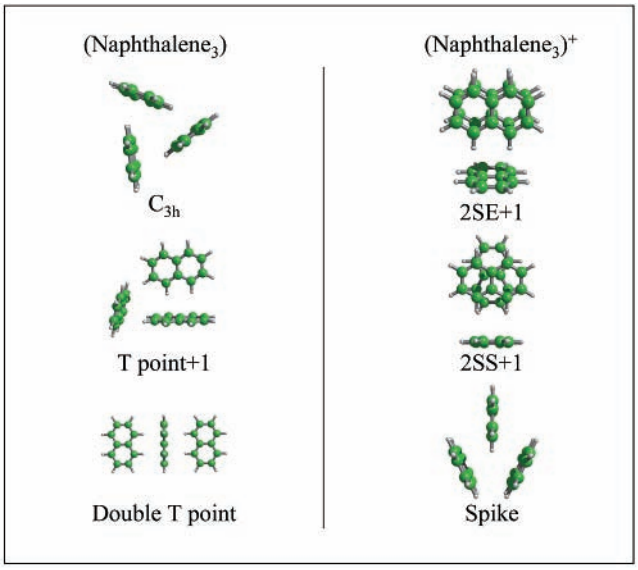

Figure 8. Structures of the most relevant minima on the (naphthalene$_3$) and (naphthalene$_3$)$^+$ PES (Tables 8 and 9).

naphthalene tetramer[67−70] hints at four symmetry-inequivalent sites. Most authors acknowledge a low-symmetry herringbone structure (which occurs in crystals containing naphthalene-like molecules[71]), although they admit that it should result, strictly speaking, in only two different site types. From our point of view, we find the global minimum to be devoid of symmetry. The two following minima, respectively C_2 and C_{2h}, feature two different symmetry-inequivalent sites. All higher minima stem from (naphthalene$_3$) or (naphthalene$_2$) building blocks.

IV.2.8. Naphthalene Dimer through Tetramer Cations. Stationary points (Table 9 and Figures 7−9) on the naphthalene dimer cation PES closely resemble that found for the benzene dimer cation. Sandwich structures are the most stable, which hints at the importance of charge resonance. However, both the staggered and eclipsed conformers are now minima (rotational barriers between these structures will be discussed hereafter). Charge delocalization occurs equally on both moieties. The predominance of polarization over charge resonance occurs earlier on than in (benzene$_n$)$^+$: the global minimum of the trimer PES is a 2SE+1 structure, where charge delocalization only

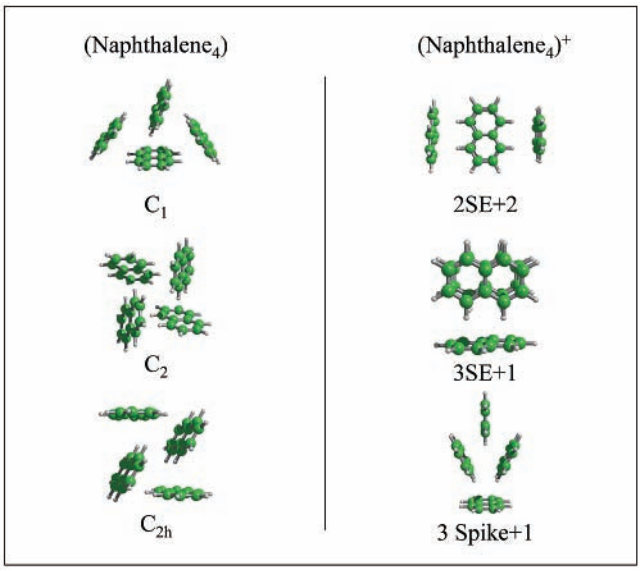

Figure 9. Structures of the most relevant minima on the (naphthalene$_4$) and (naphthalene$_4$)$^+$ PES (Tables 8 and 9).

TABLE 9: Interaction Energies (E_{Int}) and Delocalized Character of the Most Relevant Minima on the (naphthalene$_n$)+ PES, $2 \le n \le 4$ (Figures 7−9)

structure	E_{int} (kcal/mol)	delocalized character (%)
SS	−19.74	50/50
SE	−19.34	50/50
PD short axis	−14.30	50/50
PD long axis	−12.42	50/50
2SE+1	−30.42	50/50/0
2SS+1	−29.73	50/50/0
spike	−25.24	25/50/25
double T-point	−23.51	12/75/12
PD+1	−22.95	50/50/0
2SE+2	−40.71	50/50/0/0
3SE+1	−38.22	25/50/25/0
3spike+1	−35.51	25/50/25/0

involves the two stacked monomers; the first real (naphthalene$_3$)$^+$ isomer lies ca. 5 kcal/mol higher in energy. On the tetramer ion PES, no structure involving delocalization on the four monomers were found altogether; the global minimum features a sandwich-eclipsed charged dimer with two complementary neutral rings.

IV.2.9. Neutral Anthracene Clusters: Dimer through Tetramer. The PES of both charged and neutral anthracene clusters are remarkably complex, even for such small clusters as the ones we consider. In particular, a cluster of size n contains numerous minima due to the adjunction of a monomer to a size $n - 1$ cluster. In the following two paragraphs, we will restrict ourselves to typical size n structures, which we classify in families (Table 10, Figures 10−12). Clearly, a point is reached where global PES exploration becomes cumbersome and should leave place to molecular dynamics at typical jet vibrational temperatures (fifty to a hundred kelvins).

The stationary points on the dimer PES closely resemble that of the naphthalene dimer. The global minimum is T-shaped, held together by attractive dispersion and electrostatic interactions. Most other minima are stacked, attractive dispersion interactions compensating unfavorable electrostatics. To date, the question of whether the global minimum is stacked or T-shaped is still unclear.[72] The trimer PES features a triangle-shaped C_3 global minimum, compatible with previous studies;[73] the gap with consecutive trimer structures widens (6.2 kcal/mol) compared to the benzene and naphthalene trimers. These forthcoming minima are mostly 2+1 T-shaped structures. The sandwich-staggered D_{2h} structure, identified as the global minimum in other works,[15,74] lies much higher in energy. The tetramer PES is characterized by an impressive number of possible structures inside a 0.1 kcal/mol range. Particularly relevant among these are different classes of C_2-type isomers.

TABLE 10: Interaction Energies (E_{int}) of the Most Relevant Minima on the Neutral (Anthracene$_n$) PES, $2 \le n \le 4$ (Figures 10−12)

structure	E_{int} (kcal/mol)
T-point	−4.59
PD	−4.05
SS	−3.86
T-edge ⊥	−2.80
C_3	−14.14
SS D_{2h}	−7.94
C_2	−22.18

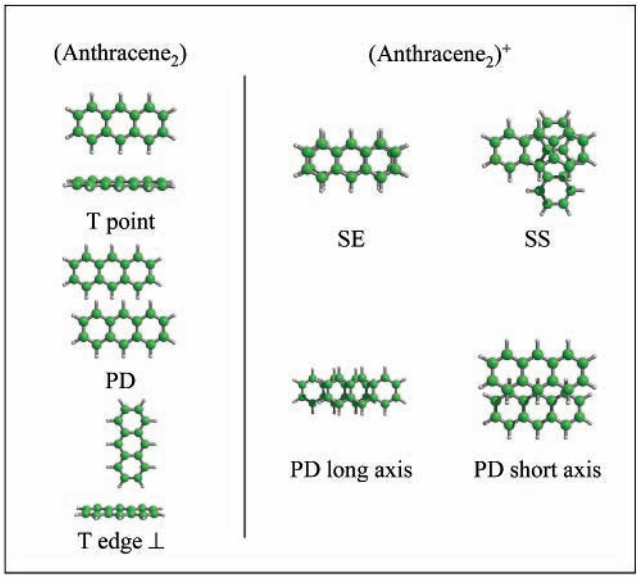

Figure 10. Structures of the most relevant minima on the (anthracene$_2$) and (anthracene$_2$)$^+$ PES (Tables 10 and 11).

IV.2.10. Anthracene Dimer through Tetramer Cations. The anthracene dimer cation's most probable structure is a sandwich-eclipsed one, with other types of stacked minima forming local minima on the PES. Spatial delocalization over the two moieties is expected in each case.

As was the case for naphthalene, polarization effects rapidly dominate over charge resonance interactions, so that the global minimum of the trimer ion PES is a 2SE+1 structure where the charge extends over two monomers. Delocalization over the three monomers can occur, but the resulting isomers are more than 5 kcal/mol higher in energy. The same trend appears in the tetramer ion, characterized by a 2SE+2 global minimum (Table 11, Figures 10−12).

IV.3. Global Trends in Small Charged Aromatic Clusters. *IV.3.1. Rotation Barriers in Charged Dimer Stacks.* As explained in the previous paragraphs, sandwich structures for charged aromatic dimers feature two different conformers: eclipsed (i.e., parallel) and staggered (resulting from the rotation of one monomer around the ring plane normal by an angle of 30° for benzene and 90° for naphthalene and anthracene). The comparison of the interconversion barriers that separate these conformers hints at the degree of rotational disorder that one can expect to find in these systems. We performed surface scans

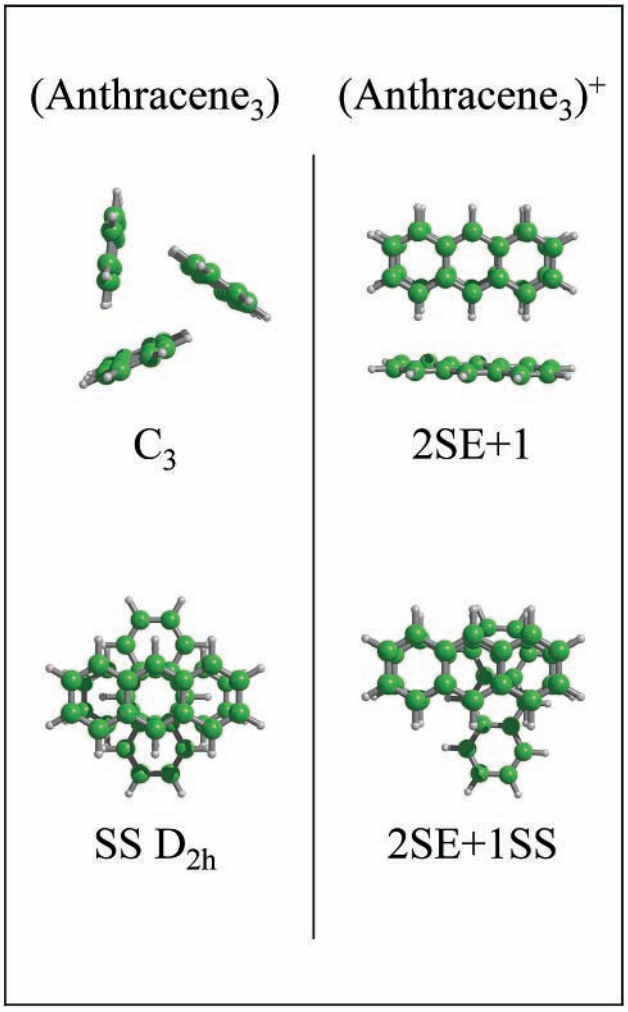

Figure 11. Structures of the most relevant minima on the (anthracene$_3$) and (anthracene$_3$)$^+$ PES (Tables 10 and 11).

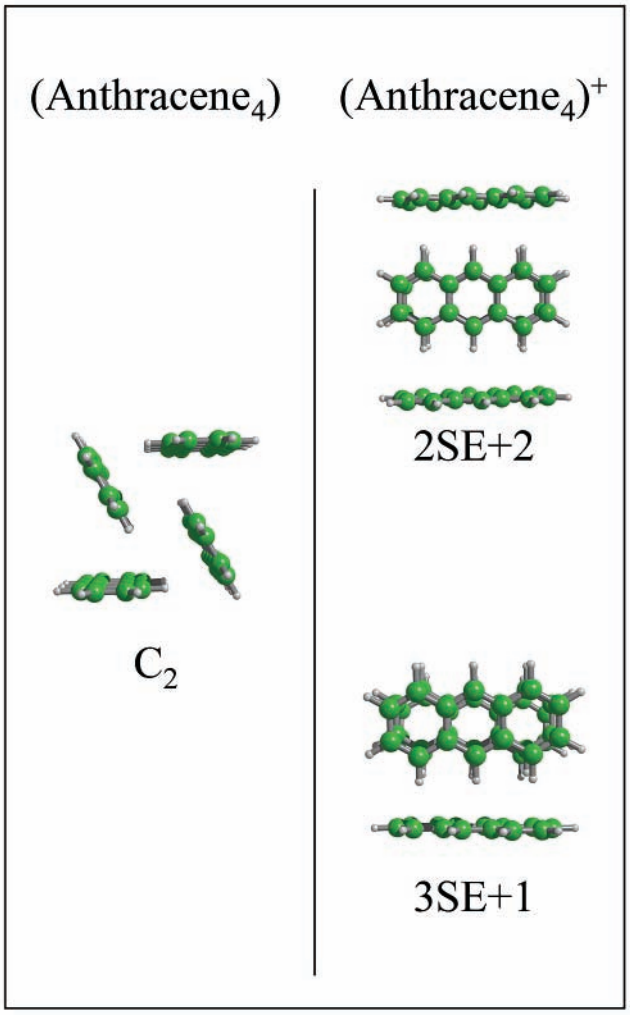

Figure 12. Structures of the most relevant minima on the (anthracene$_4$) and (anthracene$_4$)$^+$ PES (Tables 10 and 11).

along the rotation coordinate, reoptimizing the plane-to-plane distance at each step (variations of this distance with the rotation angle were found to be negligible); results are displayed on Figure 13. The barrier in the case of benzene is almost nonexistent since, as already noted, the charge-transfer interaction in these structures does not depend on the rotation angle. On the contrary, the absolute value of the overlap in the naphthalene dimer ion is maximal at 0° and 90°, and nil at 45°, and the resulting coupling element varies much more (15 kcal/mol) than the diagonal elements. Hence, the rotation barrier in this system is high and, although SS and SE structures are of similar energies, interconversion is expected to be difficult. Charge-transfer effects are also responsible for the barrier in anthracene, but the variation of the overlap is more complex, its absolute value reaching a maximum at 0° (H_{12} = 10 kcal/mol) and at 60° (H_{12} = 2.3 kcal/mol). This explains the two energy-inequivalent minima which may be seen on the plot. The barrier, albeit lower than that of the naphthalene dimer ion (ca. 9 kcal/mol), should not permit easy interconversion. Hence, the benzene dimer ion should be the only system to feature rotational disorder at typical jet temperatures.

IV.3.2. Charge Resonance vs Polarization: Where Does the Border Lie? In charged aromatic clusters, as a rule of thumb, charge-transfer effects dictate the structure of small aggregates, while for larger entities polarization effects take over. The former case results in the addition of a (generally stacked) monomer to the cluster of size $n - 1$, forming a n-molecular

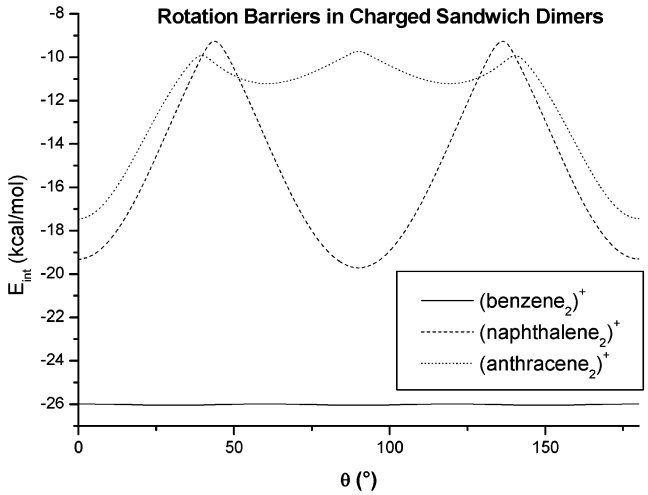

Figure 13. Variation of the interaction energy in the benzene, naphthalene and anthracene sandwich dimer ions, as a function of the rotation angle θ of the second monomer around the stack axis. Optimized interplane distances show almost no variation with θ (3.02, 3.30, and 3.54 Å for benzene, naphthalene, and anthracene, respectively).

cluster where the charge is delocalized on all monomers; the latter case is characterized by the addition of a neutral monomer to the ($n-1$)-sized cluster, with no alteration to this cluster's charge delocalization properties. As mentioned in the previous

TABLE 11: Interaction Energies (E_{int}) and Delocalized Character of the Most Relevant Minima on the (Anthracene$_n$)$^+$ PES, $2 \leq n \leq 4$ (Figures 10−12)

structure	E_{int} (kcal/mol)	delocalized character (%)
SE	−17.48	50/50
SS	−14.73	50/50
PD long axis	−13.84	50/50
PD short axis	−13.45	50/50
2SE+1	−30.73	50/50/0
2SE+1SS	−25.23	36/47/17
2SE+2	−42.89	0/50/50/0
3SE+1	−39.34	48/26/26/0

paragraphs, polarization effects become dominant from $n = 4$ in benzene, and $n = 3$ in naphthalene and anthracene, polarizabilities increasing with molecular size. The additional neutral monomer may be placed at different near-equivalent sites with regard to the $(n - 1)^+$ group, progressively generating a neutral shell around the charged cluster core; this explains the rise in the number of isomers as cluster dimensions grow. As a comparison, the charge resonance−polarization border was found to lie at $n = 3$ or 4 in charged xenon clusters[75] and at $n = 3$ in ionized argon aggregates.[76] In all these cases, the extent of charge delocalization is quite limited.

IV.3.3. Evolution of the Adiabatic-Vertical Ionization Potential Difference. For each of the aforementioned clusters, adiabatic and vertical ionization potentials were calculated. The vertical ion was obtained by a single-point calculation at the neutral global minimum geometry. Two limit cases were considered for the adiabatic ion: the "closest" ion (obtained by allowing the neutral structure to relax to the closest-lying attraction basin on the ion PES) and the "global" ion (i.e., the global minimum on this PES). Results are presented in Table 12.

For a given cluster size, adiabatic and vertical IP differences decrease in the series benzene−naphthalene−anthracene. This is due to the fact that, for naphthalene and anthracene, common structures exist for both the neutral and the ionic states, whereas in benzene there is a clear dichotomy between neutral (T-shaped) and charged (stacked) structures. The dispersive forces that bind neutral stacks increase from benzene to anthracene, up to a point where they are able to counteract the repulsive electrostatic interactions. On the contrary, for a given species, the IP difference increases as the aggregation number grows. This is not surprising for such small charged clusters, in which most monomers (2 or 3 out of 4) participate in the delocalization of the charge. Nevertheless, we mentioned that the importance of charge-transfer interactions rapidly decreases, so that for very large aggregates a negligible part of the structure will be involved in reorganization upon ionization. Hence, the IP difference is expected to converge toward a value typical of the reorganization energy of the ionic cluster core.

The "closest" and "global" adiabatic ions were found to differ in all cases. This does not come as a surprise. Small clusters feature such a structural difference between neutral and charged geometries that the two corresponding points on the ion PES lie very far from each other, the probability of encountering a local minimum between them thus being very high. Larger clusters are characterized by an important number of local minima, with the same consequence.

Finally, Table 12 compares calculated adiabatic IPs in benzene clusters to the experimental values reported by Krause et al.[77] and Nishi et al.[78] Our "closest" value for the dimer is in relatively good agreement with both experimental determinations. However, as n grows, Krause's values tend to stagnate and the gap with our results widens. Krause et al. discuss that low ionization intensities, as well as selectivity issues for larger clusters, might mitigate their results; however, it would be unfair not to mention that the theoretical determination of adiabatic IPs has its own difficulties, since it requires a good description of a whole area of the PES, and not only its minima.

IV.4. Charge Delocalization vs Polarization in Stacked Clusters. Among the different trends discussed above, the polarization vs charge delocalization competition in ionic clusters was proved to have a dominant influence over cluster structures and properties. Its manifestation in larger clusters thus seemed of interest. Unfortunately, the incentive for global exploration of a potential energy surface diminishes as the aggregation number grows, because of the exponential rise of the number of near-degenerate minima. We decided to restrict our study to the stacked class of isomers, which brings down the number of degrees of freedom per monomer from six to two (namely, translation along and rotation about the stack axis). As previously noted, although stacked structures dominate in small charged aromatic aggregates, their occurrence and stability tend to decrease for larger clusters, up to the point where they might not even be minima. Nevertheless, such constrained geometries are not devoid of interest: variations upon this theme include liquid crystals, allotropic varieties in solids (i.e., graphite), DNA helices, molecular wires, etc.

Stacked clusters of benzene (up to $n = 15$), naphthalene (up to $n = 13$) and anthracene (up to $n = 10$) were constructed and submitted to constrained optimization.

IV.4.1. Extent of the Charge Delocalization. The model Hamiltonian approach, which describes the supersystem in the basis of its monomers' states, bears close resemblance to the exciton theory. Stack eigenstates shall hence be studied using tools derived from exciton studies.[79]

The participation of a given monomer M_i to the charge delocalization phenomenon is most easily described, in the framework of our model, by the magnitude of the coefficient of the supersystem eigenvector associated with the valence bond form $(M_1M_2...M_i^+...M_n)$. Alternately, the number of coherently

TABLE 12: Computed and Experimental (exptl) Adiabatic and Vertical Ionization Potentials (kcal/mol) in Small Aromatic Homoclusters

cluster	adiabatic IP (closest)	adiabatic IP (global)	vertical IP	difference (closest)	difference (global)	adiabatic IP (exptl)
$(benzene)_2$	197.3	189.1	206.3	9.0	17.2	199.5[77] 196.7[78]
$(benzene)_3$	190.2	183.9	203.7	13.4	19.7	197.9[77]
$(benzene)_4$	188.5	180.9	203.1	14.6	22.2	197.2[77]
$(naphthalene)_2$	176.7	171.3	179.9	3.2	8.6	
$(naphthalene)_3$	172.6	167.5	178.7	6.1	11.3	
$(naphthalene)_4$	167.5	162.7	174.2	6.7	11.5	
$(anthracene)_2$	162.8	158.9	163.8	1.0	4.9	
$(anthracene)_3$	160.1	155.2	163.4	3.2	8.1	
$(anthracene)_4$	157.2	151.1	161.3	4.1	10.2	

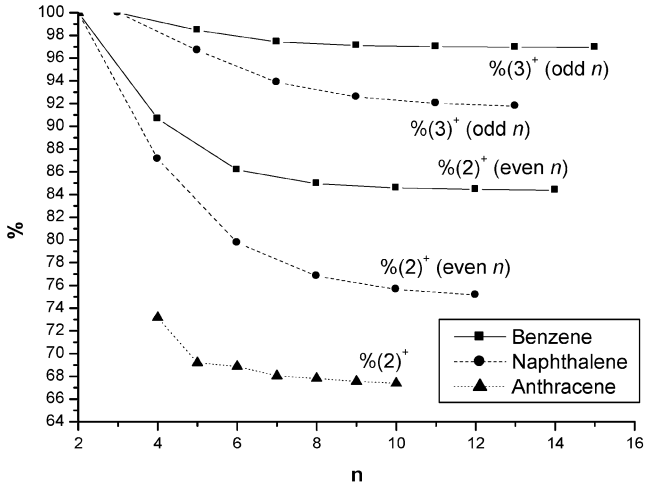

Figure 14. Contribution of the two (2^+) or three (3^+) central monomers (bearing the major part of the charge) to the global ground-state wave function of benzene, naphthalene and anthracene stack ions, as a function of the number *n* of monomers in the stack.

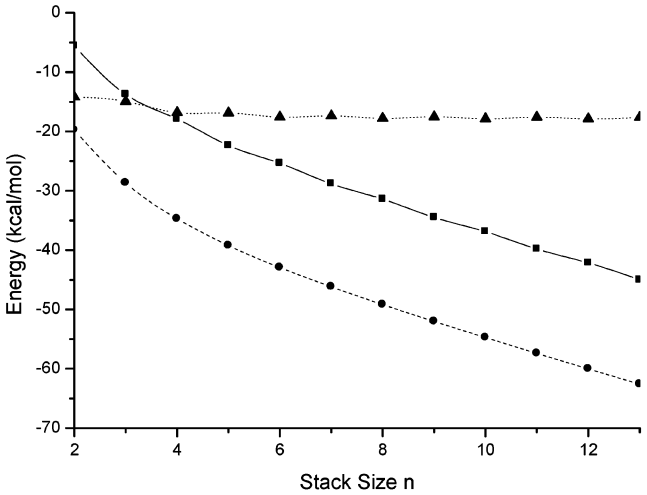

Figure 15. Global energy of stacked naphthalene ions, with charge-transfer interactions enabled (circles and dashes) or disabled (squares and continuous line), as a function of the aggregation number *n*. The difference between the two terms represents the stabilization due to charge resonance, and is also plotted (triangles and dots).

coupled monomers in a supersystem eigenstate may be expressed using a simple "participation ratio" model:[80]

$$L_k = \sum_{\text{monomers } m} [\sum_{\text{states } i} (C^i_{k,m})^2]^2 \qquad (7)$$

where the participation ratio $1/L_k$ (PR) is directly related to the number of monomers involved in the *k*th supersystem eigenstate, and C^i_{km} is the (normalized) eigenvector coefficient for monomer *m* in its *i*th state (as a reminder, two different ionic states have to be considered for the benzene monomer).

For all systems, the PR indicates that two to three monomers participate to the supersystem ion. However, this only reflects a mean trend. For benzene and naphthalene, delocalization occurs over two or three monomers for even or odd values of *n*, respectively, while for anthracene delocalization occurs mostly on two moieties. This can be seen by plotting the contribution of the $(2)^+$ or $(3)^+$ motif to the entire eigenstate (Figure 14). Albeit large, this contribution in benzene and naphthalene decreases monotonically with *n*, traducing a slight delocalization on other monomers. Convergence is reached for $n = 8$ in benzene, and $n = 10$ in naphthalene. The case of anthracene is peculiar: as already mentioned, delocalization involves mostly 2 monomers but never goes beyond 4 units: the contribution of the $(4)^+$ motif equals 100% for every $n \geq 4$.

IV.4.2. Stack Geometries. The issue of stack geometries is closely related to that of charge delocalization, since it dictates the magnitude of the overlap integrals used as a model for charge-transfer interactions.

Benzene and naphthalene stacks feature a sandwich-staggered structure, with a rotation of 30° and 90° around the stack axis from one building block to the next, respectively. The distance between consecutive monomers vary from typical ion-stack distances in the $(2)^+/(3)^+$ motifs to typical neutral-stack distances (ca. 1 Å longer) for outer monomers. This justifies the rapid but continuous decrease of off-diagonal elements and, hence, of charge delocalization. On the contrary, anthracene stacks feature a sandwich-eclipsed $(4)^+$ group surrounded by sandwich-staggered monomers. The overlap between HOMOs in staggered anthracene dimers are nil, which explains the sudden stop in charge delocalization outside the $(4)^+$ motif: polarization and charge-transfer interactions in anthracene stacks are mutually exclusive. This was not the case for benzene (for which the charge resonance effect depends only on the plane-to-plane distance) or naphthalene (for which a 90° rotation angle will accommodate both electrostatic and charge-transfer interactions).

IV.4.3. Polarization vs Charge Resonance. We come back to the polarization vs charge-transfer competition, whose importance was stressed throughout this work. A quantitative assessment of both terms may be computed. Single-point energies were determined for the optimized stack geometries, with the charge localized on the central monomer, and were compared with the corresponding charge-transfer-inclusive calculations. The difference between the two figures is the stabilization originating from charge delocalization. As can be seen on Figure 15, it does not vary much as *n* grows, with a mean value of −20 kcal/mol for benzene, −16 kcal/mol for naphthalene and −12 kcal/mol for anthracene. Although dominant in small clusters, it is rapidly caught up by the other effects (among which polarization is paramount); this occurs as soon as $n = 3$ and explains the aforementioned limited delocalization behavior.

IV.4.4. Excited States of Ion Stacks. The delocalized behavior of the ion stack excited states are compared with that of the ion ground state on Figure 16, via their participation ratio and the magnitude of the corresponding eigenvector coefficients. In the case of benzene and naphthalene, these states display a more delocalized character than the ground state: for higher excited states, the charge is able to reach the limits of the stack. The monomers bearing the greater part of the charge are different from those of the ground state and depend on the parity of the excited-state index. This "harmonic" behavior is due to the regularity of the stack structure. In anthracene the situation is far more complex, due to the presence of three distinct zones (a SE area surrounded by two SS areas). Low-index excited states tend to involve the central SE area, while higher excited states are located in either one of the SS zones and display strictly localized behaviors (owing to null coupling elements).

Excitation energies are represented on Figure 17. Beyond a sufficiently large value of *n*, additional monomers do not affect the properties of either the ground or the excited states, so that the corresponding excitation energy converges. Naturally, this process is slower for higher excited states whose delocalized characters are more extensive. In the case of naphthalene and anthracene, the first excitation energy converges toward a value

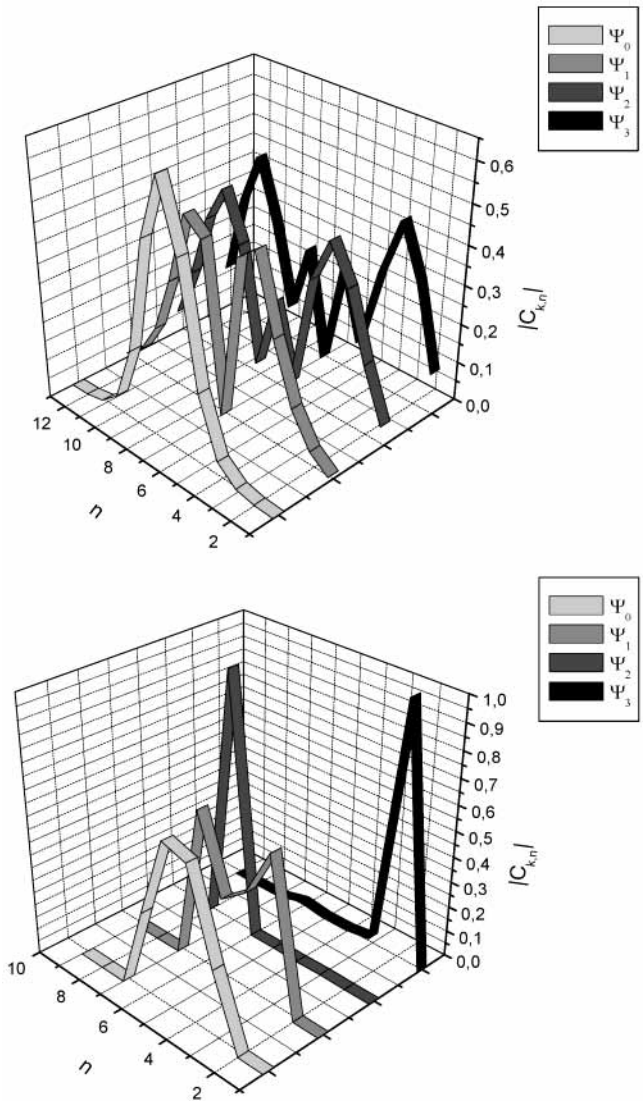

Figure 16. Topography of the ground state (Ψ_0) and the first three excited states (Ψ_1 to Ψ_3) of typical naphthalene (above) and anthracene (below) stack ions. The coefficients $C_{k,n}$ denote the contribution of monomer n to normalized eigenstate k.

of ca. 10 kcal/mol, which is typical of high-energy vibrational modes, and could lead to experimental mismatch between the electronic and vibrational excited state of the ion stacks.

V. Conclusion and Perspectives

Notwithstanding the theoretical difficulties that arise when attempting to account for charge-transfer interactions, the present work aims at proving that they may be correctly described using a simple model, compatible with global potential surface exploration or molecular dynamics simulations. Its application to charged aromatic homoclusters reveals interesting trends on the structure and electronic properties of these systems, such as the charge resonance vs polarization competition. Remarkably few studies deal with charge-transfer phenomena in aromatic aggregates; we hope that this work will provide an incentive for future works in this domain.

The limits of global potential energy surface exploration at 0 K for multidimensional or complex cases has been highlighted throughout this study; it suggests, as the most obvious extension to the present work, to utilize molecular dynamics simulations to characterize the coupling between charge delocalization and intermolecular vibration as a function of temperature. This may

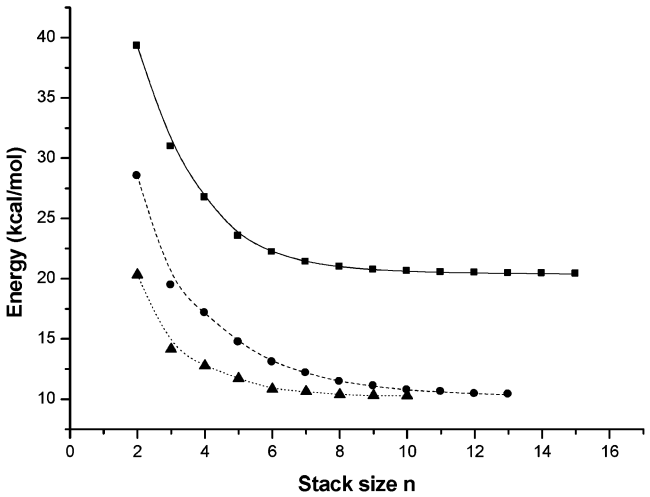

Figure 17. Excitation energies corresponding to the first excited state of benzene (squares and continuous line), naphthalene (circles and dashes) and anthracene (triangles and dots) stack ions, as a function of the aggregation number n.

be achieved by conducting the simulation on the PES corresponding to the lowest adiabatic state at each geometry. However, a more realistic description would have to take into account possible switches between adiabatic states in regions where several of these come in close vicinity (i.e., zones of avoided crossings), thus accounting for nonradiative transitions such as the ones that occur, for example, during the relaxation of an initially excited charged aggregate through internal conversion. To this effect, we are currently implementing a trajectory surface hopping formalism. Molecular dynamics simulations with electronic transitions should yield valuable insight into charge-transfer phenomena, and provide further proof of the interest of simple yet accurate potentials as tools for the study of complex systems.

Acknowledgment. The authors would like to express their gratitude to Jean-Pierre Flament for valuable information on overlap integral derivatives, as well as to Fernand Spiegelman, Tomas Baer, François Piuzzi, and Michel Mons for advice and orientation.

References and Notes

(1) Hunter, C. A.; Sanders, J. K. M. *J. Am. Chem. Soc.* **1990**, *112*, 5525.
(2) Cabarcos, O. M.; Weinheimer, C. J.; Lisy, J. M. *J. Chem. Phys.* **1998**, *108*, 5151.
(3) Kim, K. S.; Tarakeshwar, P.; Lee, J. Y. *Chem. Rev.* **2000**, *100*, 4145.
(4) Woon, D. E.; Dunning, T. H. *J. Chem. Phys.* **1994**, *100*, 2975.
(5) Dunning, T. H. *J. Phys. Chem. A* **2000**, *104*, 9062.
(6) Tsuzuki, S.; Uchimaru, T.; Tanabe, K. *J. Mol. Struct.* **1994**, *307*, 107.
(7) Hobza, P.; Selzle, H. L.; Schlag, E. W. *J. Am. Chem. Soc.* **1994**, *116*, 3500.
(8) Jaffe, R. L.; Smith, G. D. *J. Chem. Phys.* **1996**, *105*, 2780.
(9) Meijer, E. J.; Sprik, M. *J. Chem. Phys.* **1996**, *105*, 8684.
(10) Hobza, P.; Selzle, H. L.; Schlag, E. W. *J. Phys. Chem.* **1996**, *100*, 18790.
(11) Braida, B.; Hiberty, P. C. *J. Phys. Chem. A* **2000**, *104*, 4618.
(12) Braida, B.; Lauvergnat, D.; Hiberty, P. C. *J. Chem. Phys.* **2001**, *115*, 90.
(13) Braida, B.; Hiberty, P. C.; Savin, A. *J. Phys. Chem. A* **1998**, *102*, 7872.
(14) Smith, G. D.; Jaffe, R. L. *J. Phys. Chem.* **1996**, *100*, 9624.
(15) White, R. P.; Niesse, J. A.; Mayne, H. R. *J. Chem. Phys.* **1998**, *108*, 2208.
(16) Niesse, J. A.; Mayne, H. R. *J. Phys. Chem. B* **1997**, *101*, 9137.
(17) Spirko, V.; Engvist, O.; Soldan, P.; Selzle, H. L.; Schlag, E. W.; Hobza, P. *J. Chem. Phys.* **1999**, *111*, 572.

(18) Dang, L. X. *J. Chem. Phys.* **2000**, *113*, 266.
(19) Jortner, J.; Bixon, M.; Langenbacher, T.; Michel-Beyerle, M. E. *Proc. Natl. Acad. Sci. U.S.A.* **1998**, *95*, 12759.
(20) Voityuk, A. A.; Rosch, N.; Bixon, M.; Jortner, J. *J. Phys. Chem. B* **2000**, *104*, 9740.
(21) Voityuk, A. A.; Jortner, J.; Bixon, M.; Rosch, N. *J. Chem. Phys.* **2001**, *114*, 5614.
(22) Derepas, A. L.; Granucci, G.; Brenner, V.; Dognon, J.-P.; Millie, P. *Phys. Chem. Chem. Phys.* Submitted for publication.
(23) Gresh, N. *J. Comput. Chem.* **1995**, *16*, 856.
(24) Brenner, V. Thesis, Université Paris XI, 1993.
(25) Brenner, V.; Millie, P. *Z. Phys. D−At. Mol. Clusters* **1994**, *30*, 327.
(26) Derepas, A. L.; Soudan, J. M.; Brenner, V.; Millie, P. *J. Comput. Chem.* **2002**, *23*, 1013.
(27) Claverie, P. *Intermolecular Interactions: from Diatomics to Biopolymers*; Wiley: New York, 1978.
(28) Vigné-Maeder, F.; Claverie, P. *J. Chem. Phys.* **1988**, *88*, 4934.
(29) Lefevre, R. J. W. *Advances in Physical Organic Chemistry*; Academic Press: New York, 1965; Vol. 3.
(30) Calaminici, P.; Jug, K.; Koster, A. M.; Ingamells, V. E.; Papadopoulos, M. G. *J. Chem. Phys.* **2000**, *112*, 6301 and references therein.
(31) Mulder, F.; Van Dijk, G.; Huiszoon, C. *Mol. Phys.* **1979**, *38*, 577.
(32) Bouvier, B.; Brenner, V.; Millié, P.; Soudan, J. M. In preparation.
(33) Kitaigorodski, A. I. *Tetrahedron* **1961**, *14*, 975.
(34) Boys, S. F. *Rev. Mod. Phys.* **1960**, *32*, 296.
(35) Garel, T.; Niel, J. C.; Orland, H.; Velikon, B. J. *J. Chem. Phys.* **1991**, *88*, 2473.
(36) Poteau, R.; Spiegelman, F. *J. Chem. Phys.* **1993**, *98*, 6540.
(37) Bertolus, M.; Brenner, V.; Millié, P.; Maillet, J.-B. *Z. Phys. D−At. Mol. Clusters* **1997**, *39*, 239.
(38) Kirkpatrick, S.; Gellet, C. D.; Vecchi, M. P. *Science* **1983**, *220*, 671.
(39) Kirkpatrick, S. *J. Stat. Phys.* **1984**, *34*, 975.
(40) Press, W. H.; Flannery, B. P.; Teukolsky, S. A.; Vetterling, W. T. In *Numerical Recipes (FORTRAN Version)*; Cambridge University Press: Cambridge, 1989; p 307.
(41) Metropolis, N.; Rosenbluth, A.; Rosenbluth, M.; Teller, A.; Teller, E. *J. Chem. Phys.* **1953**, *21*, 1087.
(42) Kumanova, M. D. *Mol. Phys.* **1972**, *23*, 407.
(43) Dunning, T. H. *J. Chem. Phys.* **1989**, *90*, 1007.
(44) *Jaguar 4.1*; Schrödinger, Inc.: Portland, OR, 1991−2001.
(45) Krishnan, R.; Binkley, J. S.; Seeger, R.; Pople, J. A. *J. Chem. Phys.* **1980**, *72*, 650.
(46) Frisch, M. J.; Trucks, G. W.; Schlegel, H. B.; Scuseria, G. E.; Robb, M. A.; Cheeseman, J. R.; Zakrzewski, V. G.; Montgomery, J. A.; Stratmann, R. E.; Burant, J. C.; Dapprich, S.; Millam, J. M.; Daniels, A. D.; Kudin, K. N.; Strain, M. C.; Farkas, O.; Tomasi, J.; Barone, V.; Cossi, M.; Cammi, R.; Mennucci, B.; Pomelli, C.; Adamo, C.; Clifford, S.; Ochterski, J.; Petersson, G. A.; Ayala, P. Y.; Cui, Q.; Morokuma, K.; Malick, D. K.; Rabuck, A. D.; Raghavachari, K.; Foresman, J. B.; Cioslowski, J.; Ortiz, J. V.; Stefanov, B. B.; Liu, G.; Liashenko, A.; Piskorz, P.; Komaromi, I.; Gomperts, R.; Martin, R. L.; Fox, D. J.; Keith, T.; Al-Laham, M. A.; Peng, C. Y.; Nanayakkara, A.; Gonzalez, C.; Challacombe, M.; Gill, P. M. W.; Johnson, B. G.; Chen, W.; Wong, M. W.; Andres, J. L.; Head-Gordon, M.; Replogle, E. S.; Pople, J. A. *Gaussian98*; Gaussian, Inc.: Pittsburgh, PA, 1998.
(47) Boys, S. F.; Bernardi, F. *Mol. Phys.* **1970**, *19*, 553.
(48) Dupuis, M.; Marquez, A.; Davidson, E. R. HONDO 95.3 from CHEM-Station; IBM Corporation: Kingston, NY, 1995.
(49) Huron, B.; Malrieu, J.-P.; Rancurel, P. *J. Chem. Phys.* **1973**, *58*, 5745.
(50) Cimiraglia, R. *Int. J. Quantum Chem.* **1996**, *60*, 167.
(51) Hariharan, P. C.; Pople, J. A. *Theor. Chim. Acta* **1973**, *28*, 213.
(52) Andersson, K.; Barysz, M.; Bernhardsson, A.; Blomberg, M. R. A.; Fleig, T.; Fülscher, M. P.; de Graaf, C.; Hess, B. A.; Karlström, G.; Lindh, R.; Malmqvist, P.-A.; Neogrady, P.; Olsen, J.; Roos, B. O.; Sadlej, A. J.; Schütz, M.; Schimmelpfennig, B.; Seijo, L.; Serrano-Andrés, L.; Siegbahn, P. E. M.; Stalring, J.; Thorsteinsson, T.; Veryazov, V.; Widmark, P.-O. *Molcas*, version 5.0; Lund University: Lund, Sweden, 2000.
(53) Kimura, K.; Katsumata, S.; Achiba, Y.; Yamazaki, T.; Iwata, S. In *Handbook of HeI Photoelectron Spectra of Fundamental Organic Molecules*; Press, J. S. S., Ed.; Halsted Press: New York, 1981; p 189.
(54) Berg, J. O.; Parker, D. H.; El-Sayed, M. A. *Chem. Phys. Lett.* **1978**, *56*, 411.
(55) Kuhn, W. F.; Lilly-Leister, D.; Kao, J.; Lilly, A. C. *J. Mol. Struct.* **1989**, *212*, 37.
(56) Kao, J.; Eyerman, C.; Southwick, E.; Leister, D. *J. Am. Chem. Soc.* **1985**, *107*, 5323.
(57) Almlöf, J.; Roos, B.; Wahlgren, U.; Johansen, H. *J. Electron. Spectrosc.* **1973**, *2*, 51.
(58) Lindner, R.; Muller-Dethlefs, K.; Wedum, E.; Haber, K.; Grant, E. R. *Science* **1996**, *271*, 1698.
(59) Arunan, E.; Gutowski, H. S. *J. Chem. Phys.* **1993**, *98*, 4294.
(60) Schaeffer, M. W.; Maxton, P. M.; Felker, P. M. *Chem. Phys. Lett.* **1994**, *224*, 544.
(61) Milosevich, S. A.; Saichek, K.; Hinchey, L.; England, W. B.; Kovacic, P. *J. Am. Chem. Soc.* **1983**, *105*, 1088.
(62) Ohashi, K.; Nishi, N. *J. Chem. Phys.* **1991**, *95*, 4002.
(63) Ohashi, K.; Nishi, N. *J. Chem. Phys.* **1993**, *98*, 390.
(64) Hiraoka, K.; Fujimaki, S.; Aruga, K. *J. Chem. Phys.* **1991**, *95*, 8413.
(65) Henson, B. F.; Venturo, V. A.; Hartland, G. V.; Felker, P. M. *J. Chem. Phys.* **1993**, *98*, 8361.
(66) Van de Waal, B. W. *Chem. Phys. Lett.* **1986**, *123*, 69.
(67) Schaeffer, M. W.; Kim, W.; Maxton, P. M.; Romascan, J.; Felker, P. M. *Chem. Phys. Lett.* **1995**, *242*, 632.
(68) Wessel, J. E.; Syage, J. A. *J. Phys. Chem.* **1990**, *94*, 737.
(69) Saigusa, H.; Sun, S.; Lim, E. C. *J. Chem. Phys.* **1992**, *97*, 9072.
(70) Saigusa, H.; Sun, S.; Lim, E. C. *J. Phys. Chem.* **1992**, *96*, 2083.
(71) Wyckoff, R. W. G. *Crystal Structures*; Interscience: New York, 1960.
(72) Chakraborty, T.; Lim, E. C. *J. Phys. Chem.* **1993**, *97*, 11151.
(73) Piuzzi, F.; Dimicoli, I.; Mons, M.; Millie, P.; Brenner, V.; Zhao, Q.; Soep, B.; Tramer, A. *Chem. Phys.* **2002**, *275*, 123.
(74) Xiao, Y.; Williams, D. E. *Chem. Phys. Lett.* **1993**, *215*, 17.
(75) Amarouche, M.; Durand, G.; Malrieu, J.-P. *J. Chem. Phys.* **1988**, *88*, 1010.
(76) Grigorov, M.; Spiegelmann, F. *Surf. Rev. Lett.* **1996**, *3*, 211.
(77) Krause, H.; Ernstberger, B.; Neusser, H. J. *Chem. Phys. Lett.* **1991**, *184*, 411.
(78) Shinohara, H.; Nishi, N. *J. Chem. Phys.* **1989**, *91*, 6743.
(79) Bouvier, B.; Gustavsson, T.; Markovitsi, D.; Millie, P. *Chem. Phys.* **2002**, *275*, 75.
(80) Marguet, S.; Markovitsi, D.; Millie, P.; Sigal, H.; Kumar, S. *J. Phys. Chem. B* **1998**, *102*, 4697.